CHAPTER 3

LABORATORY EXPERIMENTS TO EVALUATE RIFT FACTORS

The rate at which particles are transported by RIFT across a boundary depends on a number of flow, drop and soil factors:

Drop
* drop size
* drop velocity
* possibly drop shape (as per splash erosion - Ekern, 1950)

Flow
* flow velocity
* flow depth
* viscosity (not yet studied)

Soil
* particle size
* particle density
* particle shape
* cohesion

The terms for rainfall rate, drop size, and flow velocity in Eq. 2.17 relate only to the influence of these factors in determining the frequency of drop impact in the active zone (f_d, Eq. 2.11). The term h, the flow depth, occurs in Eq. 2.22 only because q_w=hu. However, interactions between drop size, flow depth and particle size influence the mass of soil lifted into the flow by the impact of a drop of size d (D_{pd}) because the erosive stress applied to the bed varies with drop size and flow depth (Palmer, 1963; Wenzel and Wang, 1970), and the reaction to the stress varies with particle size. In most situations, both D_{pd} and t'_{pd}, the effective average time p sized particles are suspended by an impact of a drop of size d, are unknown. However the product of D_{pd} and t'_{pd} can be isolated by re-arranging Eqs. 2.20 and 2.22 to give

$$D_{pd}t'_{pd} = \frac{q_{sR}[p,d]\ \pi\ d^3}{6\ R_d\ u} \qquad (3.1a)$$

or

$$D_{pd}t'_{pd} = \frac{c_R[p,d]\ \pi\ d^3\ h}{6\ R_d} \qquad (3.1b)$$

Consequently, either of these two equations can be used to determine the variation in the product $D_{pd}t'_{pd}$ in experiments where sediment transport rates or sediment concentrations have been determined together with the relevant rain and flow characteristics.

3.1 PREVIOUS EXPERIMENTS: Moss and Green (1983)

Moss and Green (1983) performed a series of laboratory experiments using rains with drops of various size to erode beds of 0.2 mm sand under flows of various depths. Figure 3.1 shows the effect of flow depth on the product $D_{pd}t'_{pd}$ when Eq. 3.1a was applied to the data from these experiments. According to Wenzel and Wang (1970), the vertical stress applied to the surface varies inversely with flow depth to the 1.8th power but $D_{pd}t'_{pd}$ remained relatively constant in flows shallower than three drop sizes (3d) in the Moss and Green experiments. Consequently, the family of curves for h<3d shown in Fig. 3.1 can be represented by

$$D_{pd}t'_{pd} = a_1\ d^{3.48} \qquad (3.2),$$

where a_1 is a constant which is 1.26×10^{-7} for 1.26 mm<d<5.2 mm. However, for flows deeper than 3d, $D_{pd}t'_{pd}$ decreases significantly as flow depth increases and the stress applied to the surface decreases. Thus, the family of curves for h>3d can be represented by

$$D_{pd}t'_{pd} = 0.372\ h^{b_1} \qquad (3.3)$$

where

$$b_1 = 9.59\ \log_{10}(d) - 10.29 \qquad (3.4)$$

when both h and d are in mm and 1.26 mm<d<5.2 mm.

FIG. 3.1

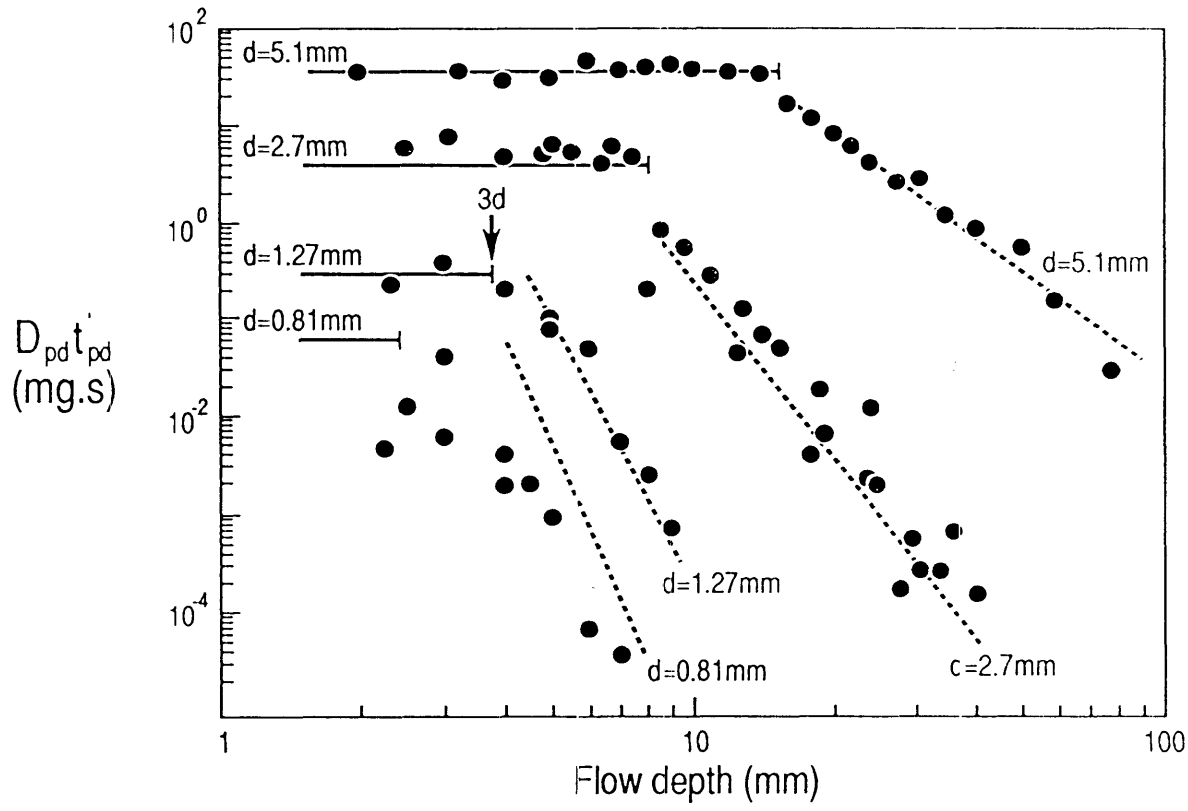

Figure 3.1. The relationship between $D_{pd}t'_{pd}$ and flow depth in the experiments of Moss and Green (1983) when drops travelling at close to terminal velocity impact flows over 0.2 mm sand. The curves shown result from Eqs. 3.2 and 3.3.

The experiments of Moss and Green (1983) include practically no data for h<3d when d=0.81 mm. However, Fig. 3.1 shows that neither Eq. 3.2 or Eq. 3.3 appear to be valid for drops of this size. This may be because small drops appear to differ from large drops in the manner they transmit the erosive stress to the bed. Drops less than about 1 mm in size cause little disruption to the surface during impact (Moss and Green, 1983).

Figure 3.1 indicates that a change in the erosive mechanism occurs when medium-to-large drops impact flows whose depth is about 3d. When medium-to-large drops impact "deep" water (h>3.5d), they carve a cavity with a depth close to 3d in the surface water (Engel, 1966; Toung and Painter, 1974). This leads to the development of above-water structures whose forms vary with drop size and impact velocity (Ghadiri and Payne, 1979; Moss and Green, 1983). The collapse of these above-water structures produces a downward flow pulse that may hit the bed with enough force to eject particles up into the water layer. The depth of the cavity varies little with impact velocity (Cai, 1989). As the water depth is reduced towards 3d, the flows generated during the collapse of the cavity may be of sufficient velocity and close enough to the bed to lift some particles up into the flow before the collapse of any above-water structure (Moss and Green, 1983). Further reductions in depth will result in the cavity reaching the bed during its excavation, the majority of particles being lifted into the flow before the collapse of the above-water structures. The direction of the pressure gradients produced in the surface water becomes more horizontal during the formation and collapse of the cavity once the cavity extends through the liquid to the bed (Macklin and Hobbs, 1969). Drops impacting very shallow flows attempt to excavate a cavity in the bed as well as the flow. Thus, although the net effect of these events is to increase the erosive stress applied to the surface underlying the flow as flow depth decreases, there is a change in the manner by which the erosive stress is applied to the surface when flows are about 3d deep.

Although a change in the manner by which the erosive stress is applied to the bed may occur when h≈3d, the change in the relationships between q_{sR} and h^{-1} for the medium-to-large drops at flow depths of about 3d in the Moss and Green experiments (Fig. 3.1) appears to result more from the change in the manner by which the erosive stress is applied than the change in the magnitude of the vertical stress applied to the soil under the layer of surface water. No substantial change can be observed in the peak pressure applied to the bed

when h=3d (Fig. 3.2). Thus it appears that some factor restricts the change in the product of D_{pd} and t'_{pd} when the vertical stress varies in those experiments where flows shallower than 3d are impacted by medium-to-large drops.

The experiments of Moss and Green (1983), Moss (1988) and Kinnell (1988) have produced results that enable the factors influencing RIFT to be examined in gross terms but insufficient knowledge about the process involved in RIFT has resulted in these experiments being inappropriate for use in a detailed examination of the effect of some of the factors on RIFT. For example, Fig. 3.3 shows the values of $D_{pd}t'_{pd}$ obtained for 2.7 mm drops when h<3d in the experiments of Moss and Green (1983) and Kinnell (1988). There is a high degree of variation in $D_{pd}t'_{pd}$ at any given value of h in both sets of data despite the flow depths being determined with an accuracy of ±0.05 mm in the Kinnell experiments.

Both Moss and Green and Kinnell used the raintower facility described by Walker *et al.* (1977). In this facility, the raindrops form on hypodermic needles spaced on a 25.4 mm grid in modules 11.2 m above the eroding surface. The angled tips of the needles used to produce the 2.7 mm drops cause the drops to fall in a slightly curved path with the drops often moving laterally some 300 mm prior to impact. Random orientation of the angled tip when the needles are inserted in the modules results in drops from adjacent needles being separated by as much as 600 mm when they reach the target, and turbulence in the air through which the drops fall helps adjacent points on the surface of the target to have equal probabilities of being impacted. Despite this, recent tests have shown that the downstream segments of targets such as those used by Moss and Green and Kinnell can receive rain at rates which may depart significantly from the average rainfall rate over the whole of the target area, and that the deviation of the rainfall rate in a segment from the average has greater temporal variation in the case of rain made up of 2.7 mm drops than in the case of rain made up of 5.1 mm drops. Evidently, variation in the impact frequency of the 2.7 mm drops in the active zone is one factor contributing to the variation in $D_{pd}t_{pd}$ observed in Fig. 3.3. The experiments reported below were made to overcome some of the inadequacies of the previous experiments and hence determine more accurately how the various factors influence RIFT and, in particular, the product of D_{pd} and t'_{pd} when h<3d.

FIG. 3.2

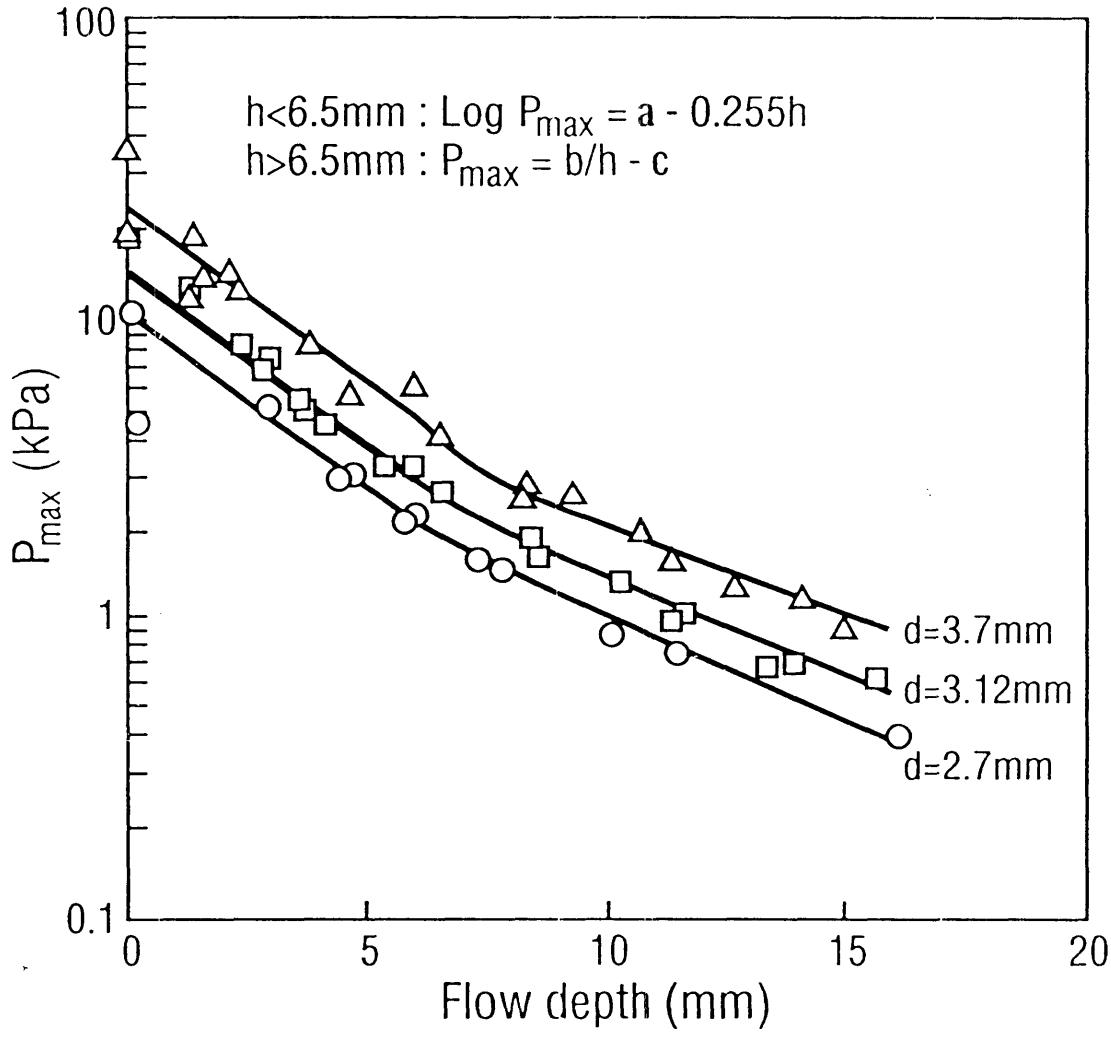

Figure 3.2. The relationships between the peak pressure exerted over a 6.7 mm diameter area and water depth when 2.7 mm to 3.7 mm drops travelling at close to terminal velocity impact static surface water deeper than 2 mm. Data from Wenzel and Wang (1970).

FIG. 3.3

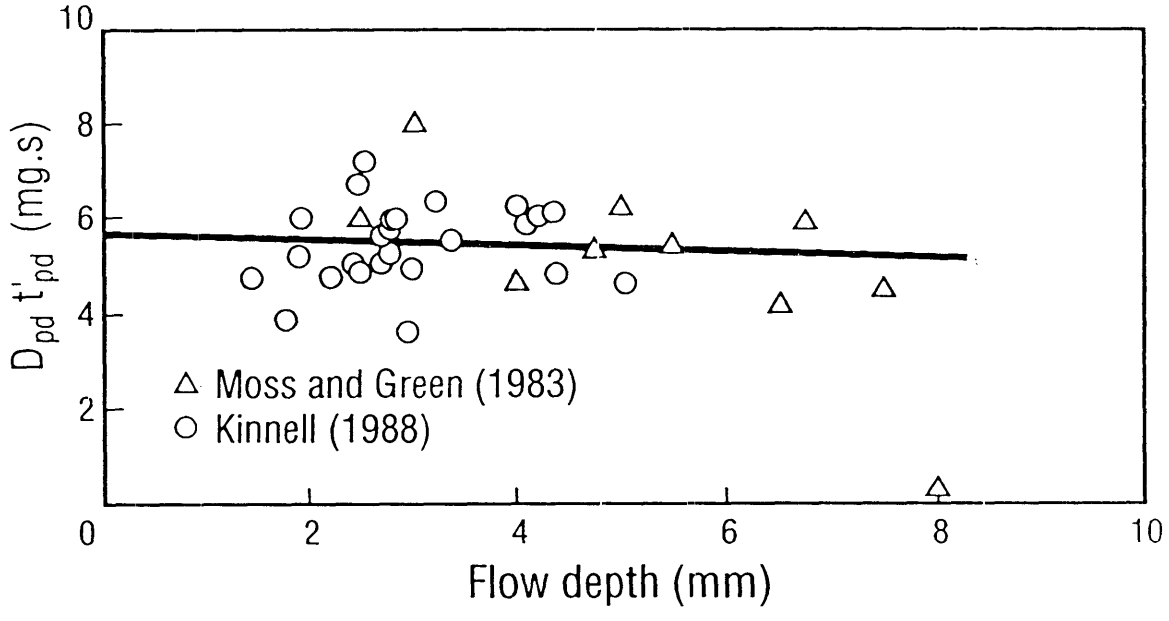

Figure 3.3. The relationship between $D_{pd}t'_{pd}$ and flow depth for 2.7 mm drops impacting flows shallower than 3d in the experiments of Moss and Green (1983) and Kinnell (1988).

3.2 CURRENT EXPERIMENTS

The primary aim of the experiments reported here is to examine the influence of flow depth, flow velocity, drop size, drop velocity, particle size and density on RIFT. The practice of keeping all but one of these factors constant as a means of examining the effect of a particular factor is adopted here. In general, four sets of experiments were conducted. In the first set, rainfall intensity was the factor varied while the other factors were maintained constant. In the second set, flow velocity was the factor varied. The purpose of these two sets of experiments was to examine the validity of the linear relationships between q_{sR} and R_d and u implied in Eq. 2.20. In the third set, flow depth was varied while drop velocity was varied in the forth set. Three drop sizes (d=2.7 mm, 3.7 mm, 5.1 mm) and four particle sizes (p=0.1 mm, 0.2 mm, 0.5 mm and 0.9 mm approx) were used. Coal particles were also used to introduce a variation in the density that was of a similar order as that observed for aggregates (1.5-1.75 Mg m^{-3}, Olson and Zobeck 1989). The purpose of these two sets of experiments was to examine the interactions between drop characteristics, particle characteristics and flow depth.

3.2.1 Equipment and Methods

The apparatus used in the current experiments (Fig. 3.4) was designed to maintain a broad flow of water over the whole width of a horizontal water-saturated target installed in the downstream end of a flume over which artificial rainfall is applied. The basic design for the apparatus was described originally by Moss and Green (1983) and was used subsequently by Moss and Green (1987) and Moss (1988). In the experiments with sand and coal reported in this thesis, the non-cohesive material was contained in a 500 mm square, 75 mm deep box. The basic principles upon which the apparatus was designed were also applied in laboratory experiments with small intact blocks of soil.

In the original design, the flow discharge resulted from the inflow at the upstream end of the box combining with the rain applied over the target area. In the current design, a "rain" bleed (Fig. 3.4) compensates for the

FIG. 3.4

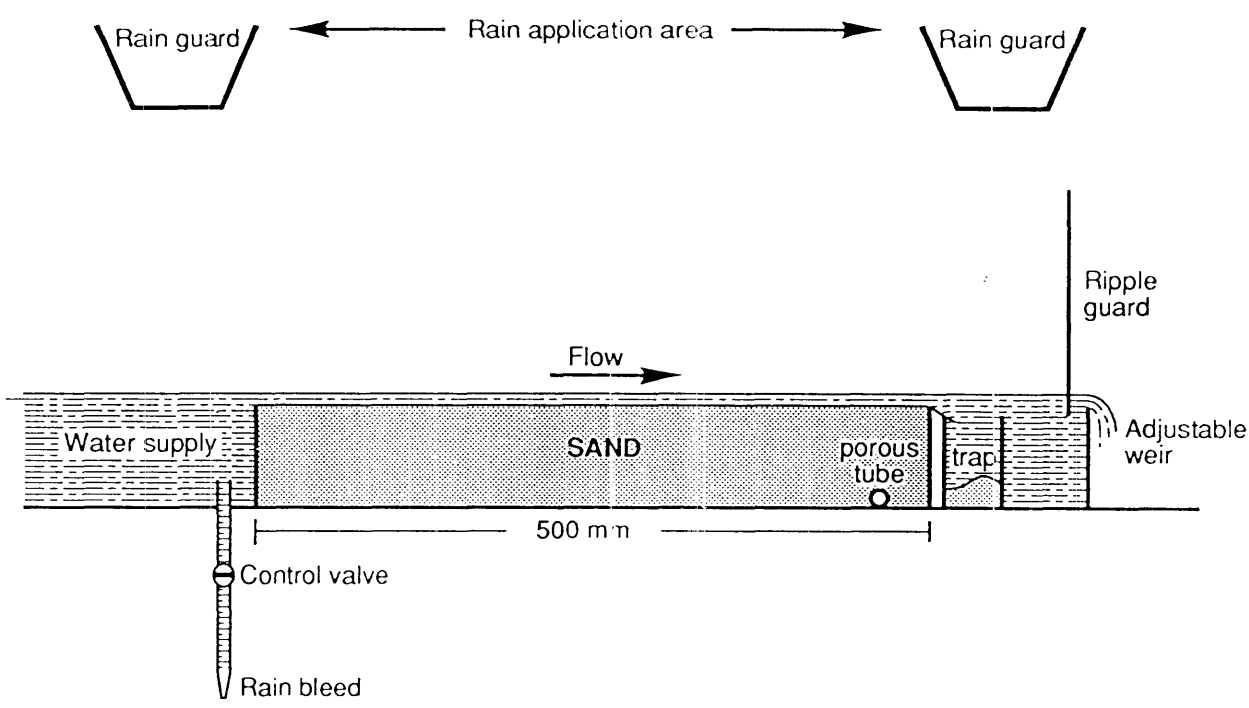

Figure 3.4 Longitudinal section of the apparatus used to study RIFT over surfaces of non-cohesive material in the current experiments.

addition of water by the rain. Flow depths are controlled by the adjustable weir at the downstream end. In all the Moss *et al.* experiments, flow depths were measured using thin graduated stakes placed vertically in the flow. In the current design, the depths of the rain-impacted flows are measured hydrostatically via a porous tube inserted horizontally along the bottom of the box 50 mm from the downstream end. This porous tube is connected to a pressure transducer (KDG Instruments Thames-Tronic 8080, 0-150 mm water gauge). This system measures the water pressure at the base of the sand and provides estimates of flow depth with an accuracy of ±0.05 mm in unimpacted flows over non-cohesive material (Kinnell, 1988). Using a different design, flow depths over less porous materials can also be measured hydrostatically (Kinnell and McLachlan, 1989).

The general procedure adopted in using this apparatus involves protecting the target from rain using a cover during the preparation stage, removing the cover to expose the target to rain consisting of uniform sized drops for the duration of the experiment (usually 10 mins), and then replacing the cover to terminate RIFT. Flow velocities below the critical velocities required to entrain the particles without the aid of raindrop impact were used in all the experiments. All the material transported across the downstream end of the target by RIFT was collected in the trap upstream of the weir. During the preparation stage, the completely saturated target was first screeded level before being temporarily drained to enable the bed elevation at 7 points across the surface at 50 mm from the downstream end to be measured using a point gauge. Flow was then gently introduced at the upstream end and the discharge and the height of the weir adjusted so as to achieve the desired flow depth and velocity when the rain was applied. When the correct conditions for the unimpacted flow were established, and the flow depth measured by the point gauge, the water pressure at the base of the sand was recorded. Once the cover was removed, flow discharge and water pressure were monitored as a means of determining the flow depth and velocity during the period when rain was applied to the target. To help ensure that flow depth and velocity conditions set prior to the application of the rain were maintained during the erosion event, the rain bleed and a ripple guard (Fig. 3.4) were used during the time when the rain was being applied to the target. Bed elevations were taken after the cover was replaced so that changes in the bed elevations that occurred during the experiment could also be determined. Rainfall rates immediately prior to and immediately after each experiment were determined from water

collected in rain gauges placed on the cover. The mean of these two measurements was assumed to provide an adequate estimate of the rainfall rate applied to the target during the experiment.

The artificial rainfall used in the experiments results from the production of pendant drops using hypodermic needles spaced on a 25.4 mm grid in the modular rainfall system described by Walker *et al.* (1977). This system enables rain of uniform drop size to be produced with drops ranging between 2.7 mm and 5.1 mm in size. The drops fall from 11.2 m so that they impact the flow at close to their terminal velocities (Laws, 1941). Lower impact velocities can be produced by reducing the height from which the drops fall.

In the majority of the experiments where RIFT provides the dominant transport mechanism, most researchers have failed to appreciate the importance of the variations in rain and flow characteristics immediately upslope of the downstream boundary of the eroding area. RIFT is a "bucket brigade" type of process, the downstream movement of the detached soil material being controlled by a series of linked events, each event being associated with a drop impact. While the chain of events some distance upstream of the boundary is important in supplying material to the active zone, it is the impacts that occur within the active zone that are crucial to the transport of the material across the downstream boundary. In the majority of experiments, drop impacts are assumed to be distributed randomly in time and space. However, this may not necessarily be so, particularly in experiments where artificial rain is generated by pendant drop formers such as used here. As can be seen from Fig. 3.5, the rainfall rate at the lower end of an eroding surface can differ significantly from the general rainfall rate measured over a larger area upstream in rain produced from this type of system. Consequently, in the experiments, the rainfall rates used for R_d were measured for the downstream 70 mm segment while the general level used (commonly about 64 mm h^{-1}) was set using the rain collected in the larger segment upstream.

In the case of 2.7 mm drops produced by hypodermic needles situated 11.2 m above the target, air currents in the raintower produce lateral movement during drop fall and this tends to produce a pseudo-random distribution of the drop impacts on the target. To help ensure that the adjacent points on the sand target have equal probabilities of being impacted, the modules were moved horizontally back and forth 250 mm at a velocity of 4.2 mm s^{-1} along the

FIG. 3.5

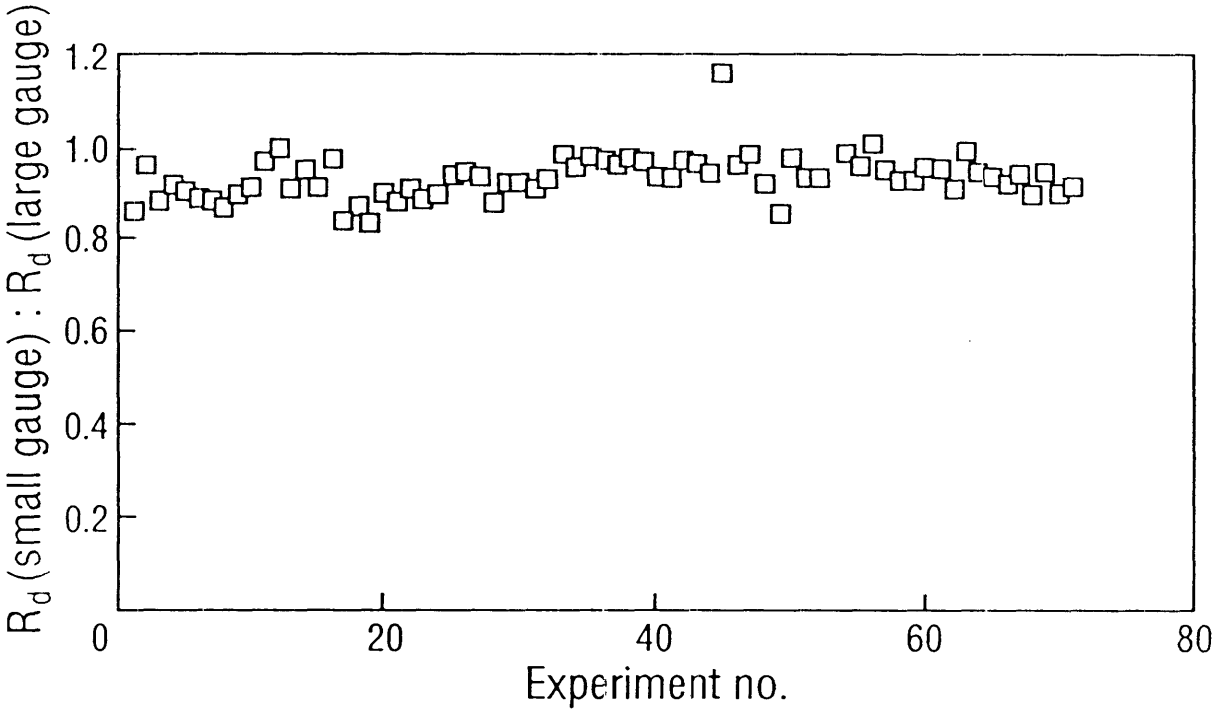

Figure 3.5. The ratio of the rainfall rate over the downstream 70 mm segment to the rainfall rate over the next upstream 420 mm segment of an eroding surface during a series of experiments made by the author using the apparatus shown in Fig. 3.4 under artificial rain produced by 23 g by 1.25 inch hypodermic needles in the raintower described by Walker *et al.* (1977). Each data point represents the mean of two measurements of 10 minutes duration separated by approximately 10 minutes for rain where d = 2.7 mm, Rd = 64 mm h^{-1} (nominal), and drop fall = 11.2 m.

direction of flow under the control of an electric motor. When compared with experiments were the modules were static, this markedly reduced the difference in the values of R_d measured before and after each experiment.

Table 3.1 shows the range of conditions applied during the experiments. Except in the case for p=0.2 mm sand which was the sand described by Moss and Green (1983), the various sized particles were obtained by sieving material rich in the required particle sizes. The source of the coal particles was ground coal. The fall velocities of the various size particles in water were measured using the top-entry technique of Puri (1934) as described by Hairsine and McTainsh (1986). In this technique, particles are introduced into the top of a 2 m column of water by the device described by Kinnell and McLachlan (Appendix II) and the mass of the particles collected at the bottom of the column at various times measured in order to determine the fall velocities of the particles.

In addition to the experiments with sand, experiments using rain-impacted flows over small (500 mm long, 250 mm wide, 100 mm deep) soil monoliths were performed in the same flume-raintower facility as used for the sand experiments. These monoliths were collected using the technique described by Kinnell and McLachlan (1989). One of the monoliths came from the bare runoff and soil loss plots on the yellow podzolic soil discussed in Section 2.4.4. The remainder came from a red earth (an association of Typic Haplargids and Typic Durarids) in a semi-arid woodland near Coolabah, N.S.W. (Kinnell *et al.*, 1990). Each monolith was eroded by four 10 minute "events", each event being at a different flow depth. The nominal flow depths were 6.9 mm. 5.6 mm, 4.3 mm, and 3.0 mm averages for the cross section where flow depth was monitored hydrostatically. Rain with 2.7 mm drops was used and the nominal flow velocity was 25 mm s^{-1}.

The experiments with the soil monoliths were similar to those with sand except a sequence of decreasing flow depth was used with each monolith. As a result, each monolith was subjected to a sequence of increasing erosive stress. Also, each monolith was subjected to 5 minutes of rain impacting a nominally 6.9 mm deep flow as a pre-treatment. This pre-treatment was used to remove any loose material and establish an initial equilibrium in the surface prior to the main set of test events. The experiments were performed early in the program prior to the development of the mechanism designed to move the

Table 3.1. Conditions used in the current experiments. x' denotes the factor being investigated, s denotes experiments in which the rainfall modules were kept static. The values in brackets in column 2 are the levels at which the respective factor was held constant. R_d was nominally 64 mm h^{-1} except where $x=R_d$.

x'	constant factors	range	levels	n
	d=2.7 mm, F=11.2 m, sand, p=0.2 mm			
R_d	h(6)u(40)	35-145	4	18
u	h(6)	19-147	6	24
h	u(40)	3-9	6	20
h	u(20)	2.9-7.6	4	16
	F=11.2 m, sand, p=0.2 mm, static rain modules			
u(s)	h(6)d(2.7)	19-155	8	35
u(s)	h(6)d(5.1)	25-162	7	20
h(s)	u(50)	2.7-11	10	48
	d=2.7,3.7,5.1 mm, F=11.2 m, 4 mm<h<3d			
p	u(20)sand	0.1-0.9	4	>50
p	u(40)sand	0.1-0.9	4	>50
p	u(20)coal	0.1-0.9	4	45
	p=0.2 mm, u=20 mm s^{-1}, 4 mm<h<3d			
v_d	d(5.1)	4.2-9	3+	35
v_d	d(2.7)	4.0-7.6	3+	55

+ Data for $D_{pd}t'_{pd}$ to h relationships at 3 levels of v_d were supplemented by experiments providing data for $D_{pd}t'_{pd}$ when h=5 mm at 2 to 3 other levels of v_d.

rain modules back and forth. Consquently, the experiments were performed with static modules. Full details of the procedure used in the experiments with the soil monoliths are presented in Kinnell *et al.* (1990).

3.3 RESULTS

3.3.1 *Bed Elevations*

An eroding surface can be considered to consist of a number of elements. When RIFT is the transport process being considered, and the extent of each element along the line of flow is equal to the distance the particles travel while they are temporarily suspended in the flow after a drop impact, a lowering of the surface within an element occurs if the ability of the drop impacts to transport material across the lower boundary of the element exceeds the rate material is transported across the upper boundary. Conversely, the surface rises if the transport rate across the upper boundary exceeds that across the lower boundary.

In the experiments using sand, minor irregularities were generated in the surface of the target because the temporal and spatial distribution of the drop impacts produced by the pendant drop forming system were not completely random when the rain modules were static. Major irregularities were observed in experiments with low impact velocities and low flow velocities (e.g., for 2.7 mm drops travelling at 3.24 m s^{-1} impacting 5 mm deep flows with u=20 mm s^{-1}) unless the modules were moved to prevent the drops from any given drop former impacting consistently in one spot.

In all experiments with surfaces made up of non-cohesive materials, a net reduction in bed elevation occurred at the upstream end of the target as the result of the inflow not bringing in material into this zone. Because the continued reduction in bed elevation reduces, and eventually eliminates RIFT, the zone of reduced elevation moves downstream until, given sufficient time, it reaches the downstream end of the target. However, in all the current experiments, the excavated zone was small. In the majority of cases, the change in the bed elevation 50 mm upstream of the downstream end of the target during the experiment was small (<0.5 mm) indicating that little net erosion or deposition occurred in this and the active zone.

3.3.2 *Rainfall Intensity (R_d) and Flow Velocity (u)*

Figure 3.6 shows the effect on q_{sR} of varying rainfall intensity (R_d) between 35 mm h^{-1} and 145 mm h^{-1} when 2.7 mm drops impact 6 mm deep 40 mm s^{-1} flows over 0.2 mm sand after falling 11.2 m from the rain modules. These drops impact at close to their terminal velocity (Laws, 1941). Figure 3.6 also shows the effect of varying flow velocity (u) between 20 mm s^{-1} and 100 mm s^{-1} when R_d is held close to 60 mm h^{-1}. Analysis of the data shown in Fig. 3.6 (Table 3.2), together with data obtained when flow depth over the 0.2 mm sand was varied when u was maintained close to a number of levels (Fig. 3.7), shows that the linear relationships between q_{sR} and R_d and u implied by Eq. 2.20 are valid for d=2.7 mm and p=0.2 mm. When the data in Figs. 3.6 and 3.7 are considered in conjunction with the data of Moss (1988, Fig. 2.3; pers comm, Table 2.1) and Walker *et al.* (1978, Fig. 2.4), it is apparent that these linear relationships apply over a wide range of drop sizes, particle sizes and flow depths.

Although the theory developed in Chapter 2 and much of the available data support a direct relationship between q_{sR} and u, data from some experiments indicate a non-linear influence of u on q_{sR}. In the case of 2.7 mm drops travelling at close to terminal velocity impacting 6 mm deep flows over 0.2 mm sand, the relationship between q_{sR} and u was non-linear when the rain modules remained stationary (Fig. 3.8) but was linear when the modules were moved back and forth (Fig. 3.7). Similar relationships were observed under the rain made up of 5.1 mm drops. These non-linear relationships are artifacts associated with the rain producing system. Subsequent measurement of the rainfall distributions over the target showed that the rainfall intensity increased with distance upstream at the downstream end of the target when the modules producing the 2.7 mm drops were kept stationary. Evidently, at least some of the increase in q_{sR} with u in Fig. 3.8 results from the spatially average impact frequency in the active zone increasing as the extent of the active zone increases with u. Some of the effects of the non-randomness in raindrop impact being overcome by the particle travel distances increasing with u may also contribute to the observed increase of q_{sR} with u, particularly in the case of rain made up of 5.1 mm drops. 5.1 mm drops are

FIG. 3.6

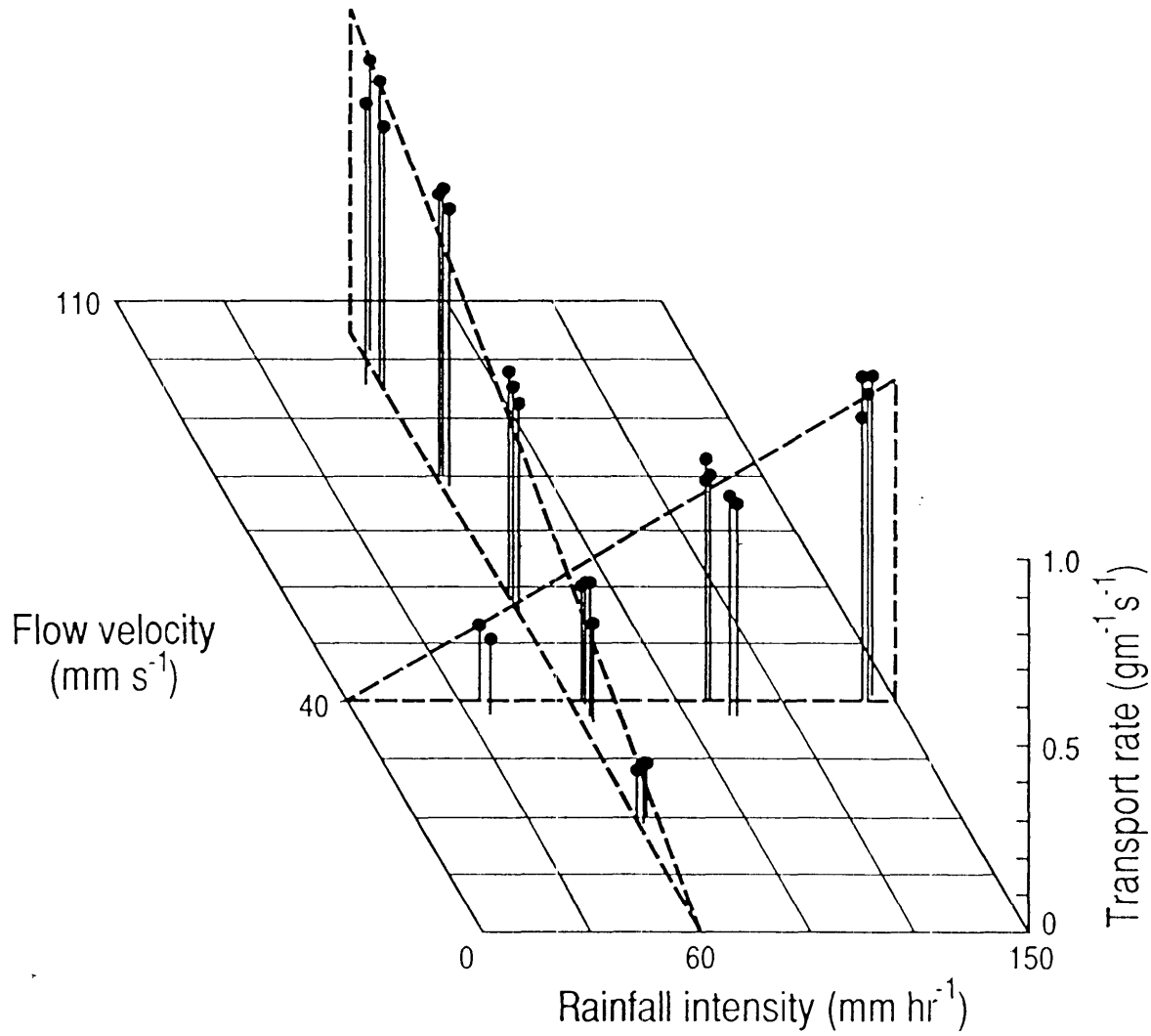

Figure 3.6. Transport rates (q_{sR}) for 0.2 mm sand obtained for d=2.7 mm, h=6 mm and $v_d \approx v_t$ (terminal velocity) when R_d was varied while u was held close to 40 mm s^{-1}, and when u was varied while R_d was held close to 60 mm h^{-1}. The variation in h was limited to 5 %.

Table 3.2. Regression analysis for the effect of rainfall intensity (R_d, mm h^{-1}), flow velocity (u, mm s^{-1}) and flow depth (h, mm) on the sediment transport rate (q_{sR}, g m^{-1} s^{-1}) for p=0.2 mm, d=2.7 mm and F=11.2 m. The values in brackets in column 2 are the levels at which the respective factor was held constant. NB. The values of u and h were maintained within 5 % of the numbers shown in parenthesis. R_d values when u,h = constant varied considerably. For R_d, the values in parenthesis are nominal.

$$q_{sR} = k' + b'X$$

X	constant factors	k'	std dev	b'	std dev	X range	n	r^2
R_d	u(40)h(6)	-0.0323	0.0313	0.00606	0.00032	35-145	18	0.955
u	R_d(61)h(6)	0.0638	0.0306	0.00737	0.000394	19-147	24	0.938
h	R_d(62)u(40)	0.8079	0.0185	-0.0840	0.002685	4.2-9.0	17	0.984
h	R_d(66)u(20)	0.4652	0.0148	-0.0521	0.002628	2.9-7.6	13	0.970

$$q_{sR} R_d^{-1} u^{-1} = k' + b'X$$

X	constant factors	k'	std dev	b'	std dev	X range	n	r^2
h	u(40&20)#	3.3E-4	7.4E-6	-3.4E-5	1.17E-6	2.9-7.6	30	0.968

Data for u=40 mm s^{-1} and u=20 mm s^{-1} combined

FIG. 3.7

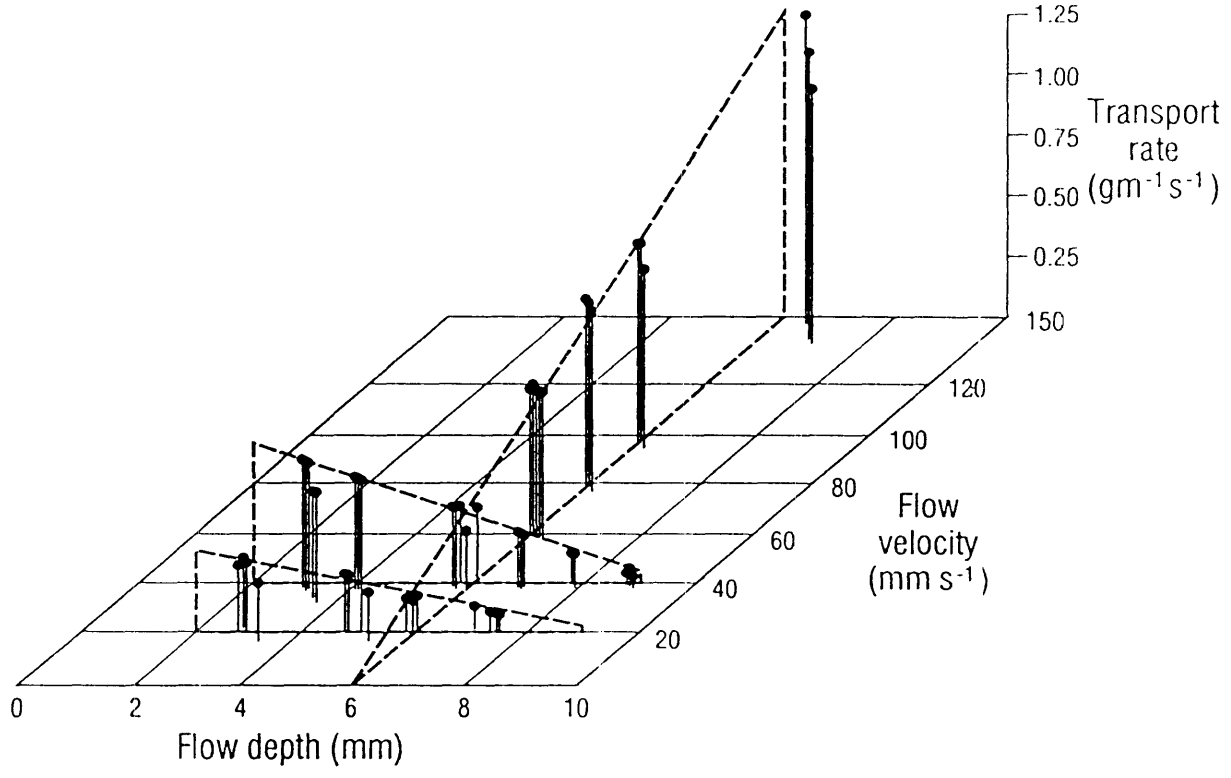

Figure 3.7. Transport rates (q_{sR}) obtained for rain with 2.7 mm sized drops impacting flows over 0.2 mm sand after 11.2 m fall when Rd = 64 mm h^{-1}, h = 6 mm, and 20 mm s^{-1} <u< 150 mm s^{-1}, and when flow depth was varied when u was held close to a number of levels. These transport rates were determined by adjusting the observed rates by the ratio of 64 mm h^{-1} to the rainfall rate measured over the 70 mm downstream segment of the target.

FIG. 3.8

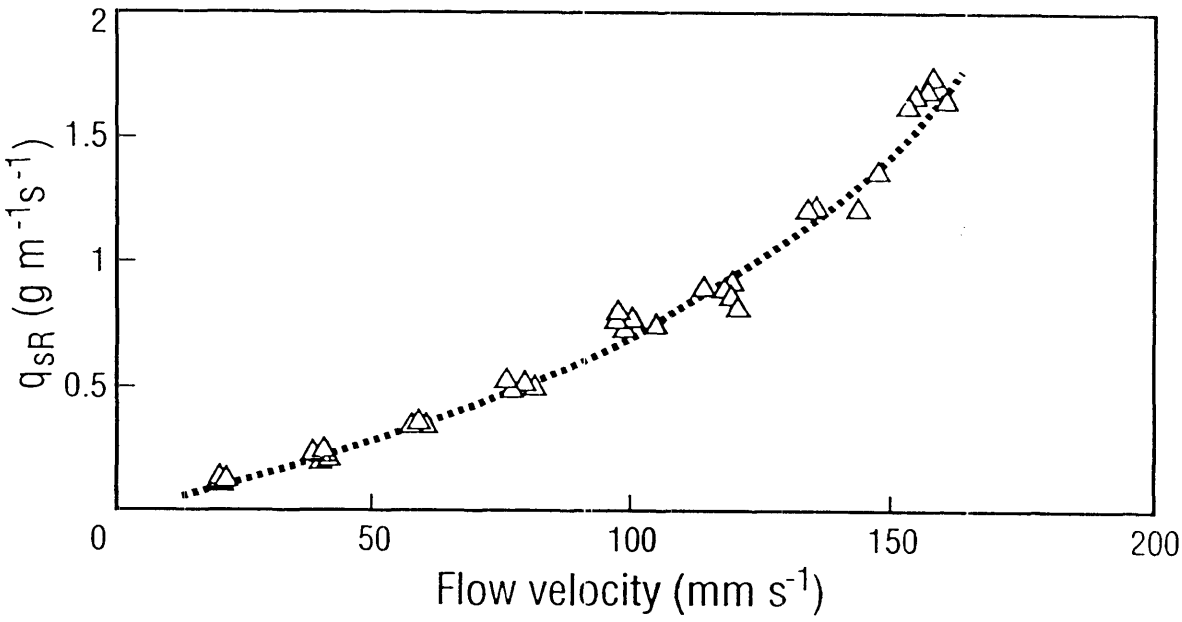

Figure 3.8. Sediment transport rates (q_{sR}) obtained for rain with 2.7 mm drops impacting flows over 0.2 mm sand after 11.2 m fall when R_d=64 mm h^{-1}, h=6 mm, and u was varied while the rain modules remained static. As in Fig. 3.7, these transport rates were determined by adjusting the observed rates by the ratio of 64 mm h^{-1} to the rainfall rate measured over the 70 mm downstream segment of the target. The variation in h was limited 5 %.

less prone than 2.7 mm drops to moving laterally under the influence of air currents during their fall to the target.

3.3.3 *Interactions between flow depth, drop size and particle size*

Because q_{sR} and $D_{pd}t'_{pd}$ are directly related to each other, Fig. 3.7 shows that, for flows with d<h<3.5d over 0.2 mm sand with 2.7 mm drops impacting at near terminal velocity, $D_{pd}t'_{pd}$ varies with h according to the equation

$$D_{pd}t'_{pd} = k_0(1 - \beta h) \qquad (3.5)$$

where k_0 is the intercept on the $D_{pd}t'_{pd}$ axis projected by the linear equation

$$D_{pd}t'_{pd} = k_0 - b_2 h \qquad (3.6).$$

and β is the inverse of the projected intercept on the h axis. It follows from Eq. 3.6 that

$$\beta = \frac{b_2}{k_0} \qquad (3.7).$$

Data obtained for 2.7 mm drops impacting flows over other sized sands (Fig. 3.9) show that the relationship given by Eq. 3.5 holds over a wide range of particle size (p) when 1.5d<h<3.5d with β not being influenced significantly by p. For h>4d, the data obtained here indicate that the relationship between $D_{pd}t'_{pd}$ and h follows the form of Eq. 3.3. Below some critical flow depth, $D_{pd}t'_{pd}$ must decline as splash becomes the dominant transport mechanism. There is evidence of a decline in $D_{pd}t'_{pd}$ when d=2.7 mm and h falls below 4 mm (Fig. 3.9). The ability of the weir to control flow depth diminishes markedly when h<4 mm and u=40 mm s^{-1}. This resulted in the experiments being limited to flows with h>2.7 mm.

Figure 3.10 shows Eq. 3.5 to also hold when the rain modules producing 2.7 mm drops remain stationary. However, when u=50 mm s^{-1}, the value of k_0 is 14 % less than that observed for the case when the modules move back and

FIG. 3.9

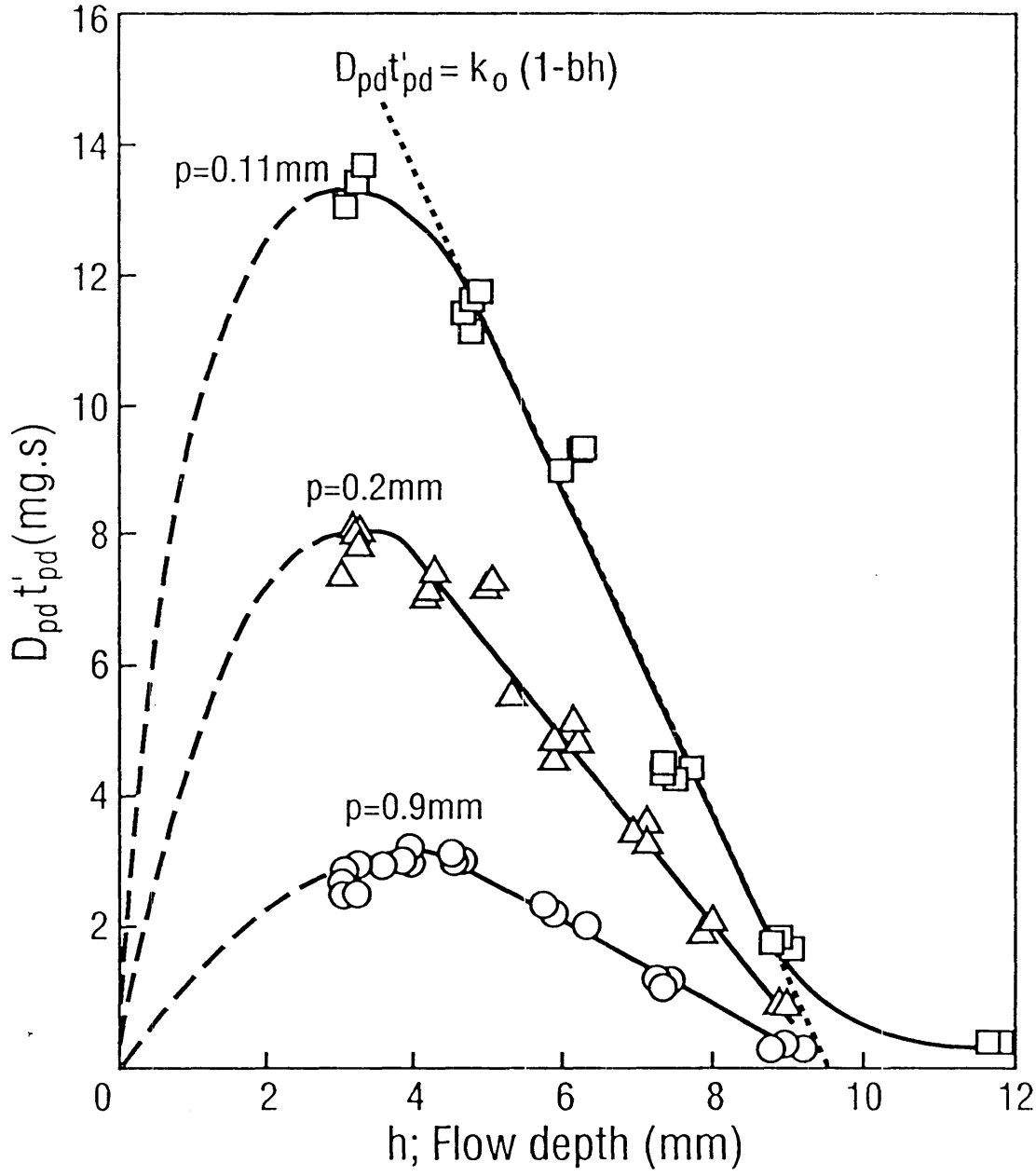

Figure 3.9. Values of $D_{pd}t'_{pd}$ obtained for R_d=64 mm h^{-1} and u=40 mm s^{-1} when 2.7 mm drops impact flows of various depths over various sized sands. Drop fall=11.2 m.

FIG. 3.10

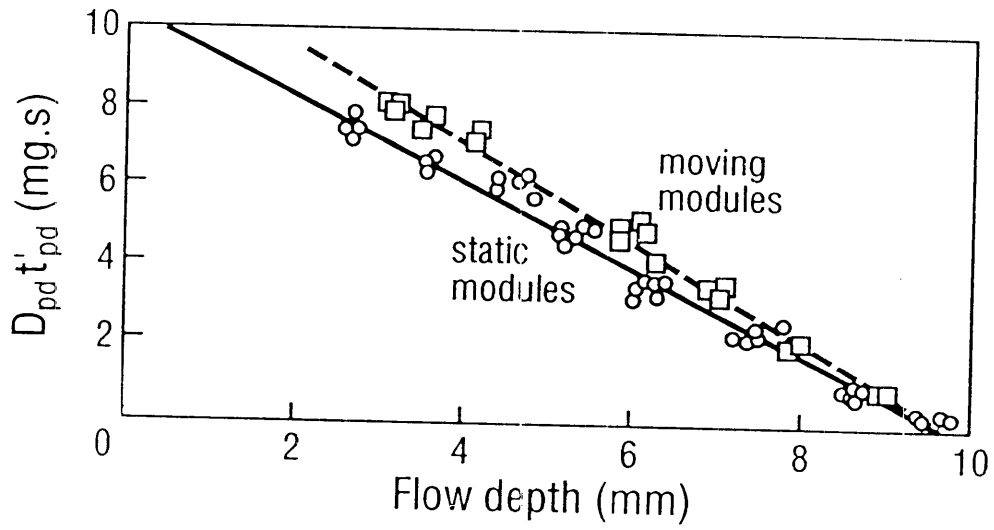

Figure 3.10. Values of $D_{pd}t'_{pd}$ obtained when 2.7 mm drops produced from mobile and static rain modules impact flows of various depths over 0.2 mm sand when u=50 mm s^{-1}. Drop fall=11.2 m.

forth. This reduction in k_0 probably results from inefficiencies in the transport system generated by the failure of some points on the surface to receive the same number of drop impacts as others.

The trends shown in Fig. 3.9 are typical for the drop sizes tested; ß remains constant while k_0 varies with particle size when drop size is held constant (Fig. 3.11, Table 3.3). Both k_0 and ß are influenced by drop size. ß shows a linear relationship (r^2=1.00) with d,

$$ß = 0.175 - 0.0260\ d \qquad (3.8),$$

whereas, except for d>2.7 mm when p=0.46 mm, k_0 can be described by (r^2=0.982)

$$\log k_0 = -0.507 - 0.616 \log p + 2.24 \log d \qquad (3.9)$$

where p (particle size) and d (drop size) are expressed in millimetres (Fig. 3.12). The 0.46 mm sand behaves according to expectations when the flows are impacted by 2.7 mm drops but behaves more and more like the 0.2 mm sand as drop size increases (Fig. 3.11). As shown in Fig. 3.13, the different behaviour of the 0.46 mm sand can also be seen by its increasing departure from

$$\log k_0 = -1.301 - 0.465 \log v_p + 2.24 \log d \qquad (3.10),$$

where v_p is the terminal velocity of fall of the particles in water (see Table 3.5), as drop size increases.

3.3.4 *Drop impact velocity (v_d)*

Drop velocity (v_d) varies with the vertical distance a drop travels after release from a drop former (Laws, 1941). In addition to the drop fall of 11.2 m, facilities were developed to vary drop fall from 1 m to 3.6 m in order to examine the effect of drop velocity on RIFT. From basic physical principles (Wang and Pruppacher, 1977) together with the drag coefficients of Wenzel and Wang (1970), 2.7 mm drops achieve a velocity close to 4.05 m s^{-1} after 1 m fall, 6.07 m s^{-1} after 3 m fall and 7.61 m s^{-1} after 11.2 m fall. The

FIG. 3.11

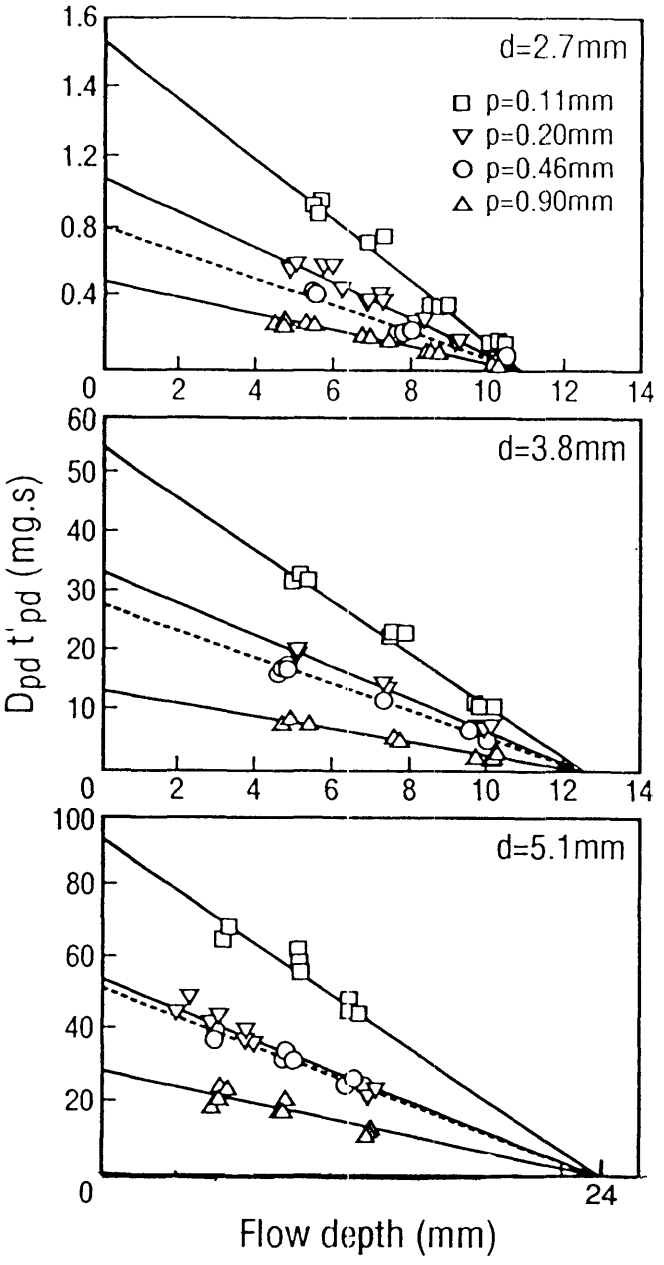

Figure 3.11. The relationships between $D_{pd}t'_{pd}$ and flow depth for the 3 drop sizes and 4 sand sizes used in the current experiments when the drops were impacting flows at close to their terminal velocities after 11.2 m fall.

Table 3.3(A). Regression analysis for the effect of flow depth (h) on $D_{pd}t'_{pd}$ for sand of various particle size (p) for flows impacted by 2.7 mm drops after falling from 11.2 m.

ANALYSIS FOR EFFECT OF FLOW DEPTH (h) ON $D_{pd}t'_{pd}$

LINEAR REGRESSION $D_{pd}t'_{pd} = k_0 - b_2h = k_0 (1 - ßh)$

p	k_0 (mg.s)	std dev	b_2	std dev	ß (mm^{-1})	h range	n	r^2
				u=20 mm s^{-1}				
0.2	12.289	0.438	1.332	0.078	0.1084	2.9-7.6	13	0.961
				u=40 mm s^{-1}				
0.11	23.347	0.810	2.462	0.121	0.1054	4.7-9.0	15	0.967
0.2	12.758	0.268	1.331	0.039	0.1043	4.1-9.0	17	0.986
0.46	11.563	0.615	1.350	0.104	0.116	4.6-6.7	5	0.977
0.9	5.991	0.122	0.636	0.018	0.1061	4.5-9.2	12	0.991

Table 3.3(B). Regression analysis for the particle size on k_0 for sand under flows impacted by drops of various size (d) after falling from 11.2 m

ANALYSIS FOR EFFECT OF PARTICLE SIZE ON k_0

NON-LINEAR REGRESSION $D_{pd}t'_{pd} = k_0 (1 - ßh)$

	d=5.1 mm u=20 mm s^{-1}			d=3.7 mm u=20 mm s^{-1}			d=2.7 mm u=40 mm s^{-1}		
	ß	std.err		ß	std.err		ß	std.err	
	0.0425	0.0017		0.0792	0.0009		0.1051	0.0010	
p (mm)	k_0 (mg.s)	std err	n	k_0 (mg.s)	std err	n	k_0 (mg.s)	std err	n
0.11	90.52	2.48	8	53.90	0.965	9	22.977	0.495	14
0.2	52.55	1.22	10	32.89	0.786	8	13.360	0.348	19
0.46	50.19	1.57	9	27.15	0.678	7	9.754	0.534	5
0.9	27.05	1.25	10	12.85	0.697	10	5.906	0.398	12
				% variance accounted for					
	97.7			99.0			97.9		

FIG. 3.12

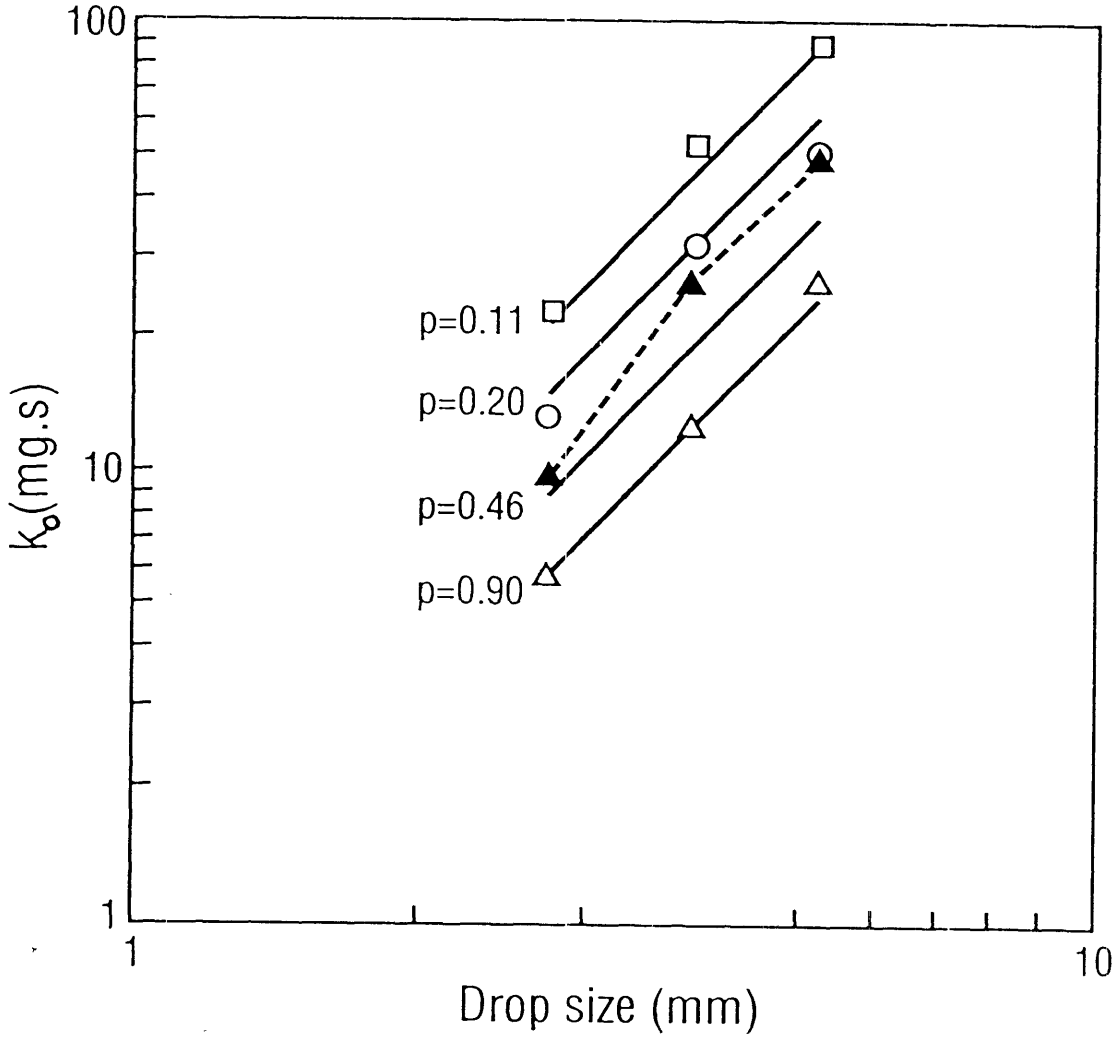

Figure 3.12. The influence of drop size (d) on k_0 in the relationships between $D_{pd}t'_{pd}$ and h shown in Fig. 3.11. The solid lines show the relationships that result from Eq. 3.9. The solid triangles the data are for p=0.46 mm.

FIG. 3.13

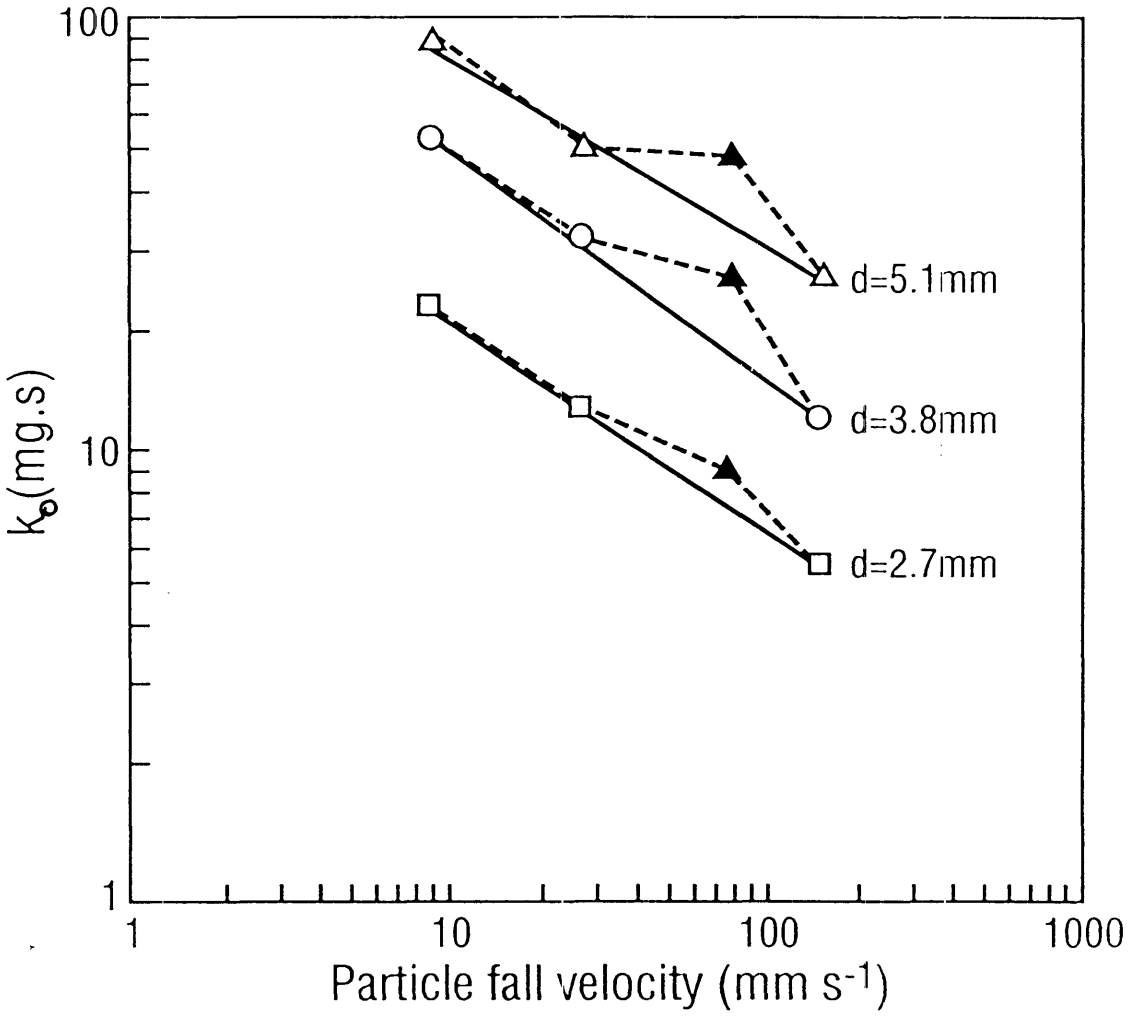

Figure 3.13. The influence of particle fall velocity (v_p) on k_0 in the relationships between $D_{pd}t'_{pd}$ and h shown in Fig. 3.11. The solid lines show the relationships that result from Eq. 3.10. The solid triangles are the data for p=0.46 mm.

corresponding velocities for 5.1 mm drops are 4.24 m s^{-1}, 6.72 m s^{-1}, and 8.95 m s^{-1}.

In terms of RIFT, Fig. 3.14(B) shows that Eq. 3.5 applies when 2.7 mm drops travelling at velocities which significantly lower than the terminal velocity for drops of this size impact flows over 0.2 mm sand. In contrast to the effect of p on $D_{pd}t'_{pd}$ for d=2.7 mm, both k_0 and ß vary with impact velocity. Similarly, Eq. 3.5 applies when 5.1 mm drops impact flows at subterminal velocity with both k_0 and ß varying with impact velocity (Fig. 3.14(A), Table 3.4). For 2.7 mm drops (Fig. 3.14(B)),

$$k_0 = 2.67v_d - 8.07 \qquad (3.11)$$

and

$$ß = 0.197 - 0.0118v_d \qquad (3.12).$$

The r^2 values for Eqs. 3.11 and 3.12 are 1.000 and 0.995 respectively. For 5.1 mm drops (Fig. 3.14(A), Table 3.4)

$$ß = 0.0852 - 0.00442v_d \qquad (3.13)$$

The r^2 value for Eq. 3.13 is 1.000. The value of k_0 for 5.1 mm drops increases non-linearly with v_d (Table 3.4). Large drops change shape during their fall from a drop former (Kinnell, 1972) and drop shape has been shown to be a factor in splash erosion (Ekern, 1950). The non-linear relationship between k_0 and v_d for 5.1 mm drops may have been caused by the variations in drop shape that occurred but that were not measured in the experiments. The dependence of k_0 and ß on impact velocity results in $D_{pd}t'_{pd}$ varying with a power of v_d at some flow depths but not at others (Fig. 3.15). Thus a simple relationship between $D_{pd}t'_{pd}$ and v_d does not hold for all flow depths. However, drop momentum (p_m) was found to be useful in the prediction of k_0 and ß when drops impact at close to their terminal velocities. Analysis of the data for drops impacting the flows over the 0.11 mm, 0.2 mm and 0.9 mm sands after 11.2 m fall gave

$$\log k_0 = 7.543 - 0.4652 \log v_p + 0.7025 \log p_m \qquad (3.14)$$

FIG. 3.14

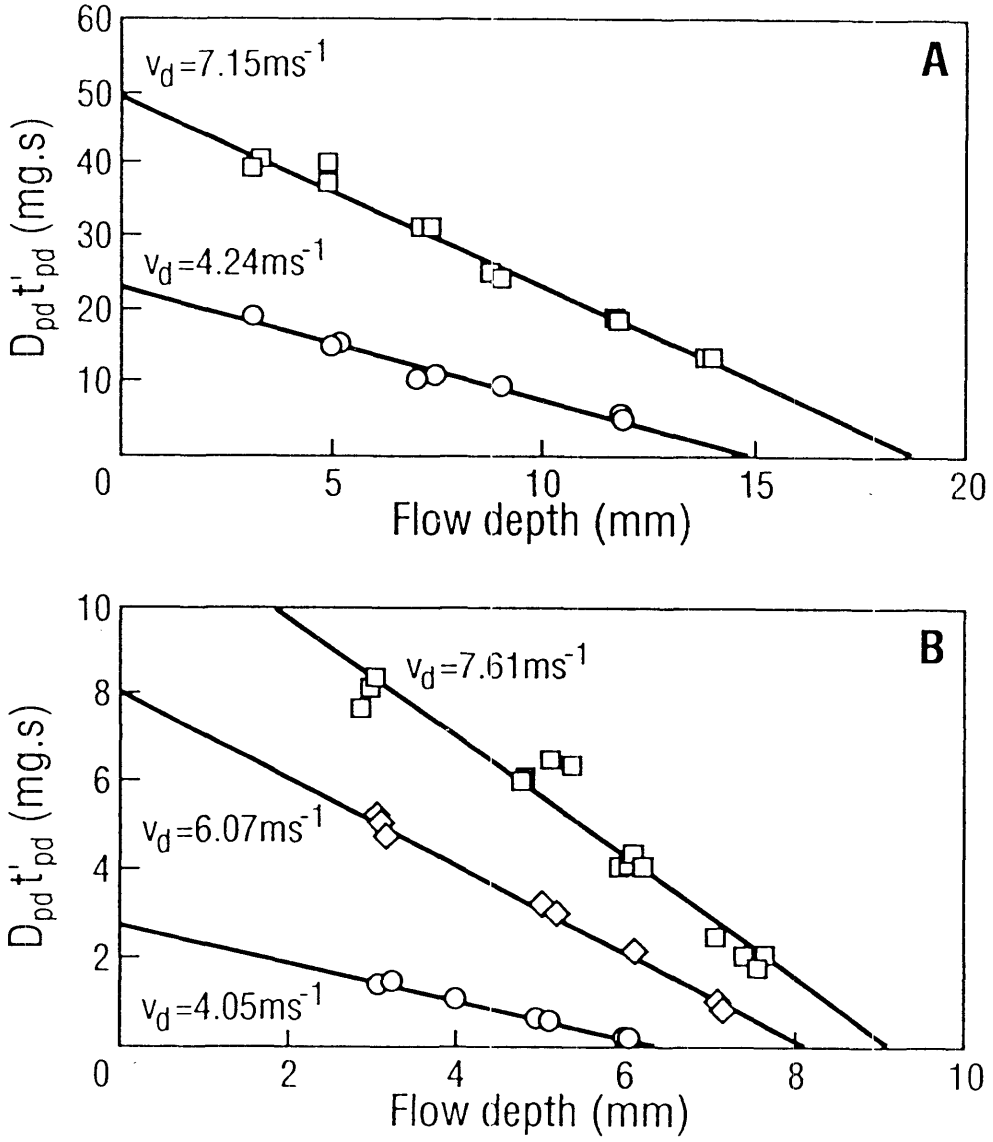

Figure 3.14. The effect of drop impact velocity on the $D_{pd}t'_{pd}$ to h relationships for (A) 5.1mm and (B) 2.7mm drops.

Table 3.4. Regression analysis for the effect of flow depth (h) on $D_{pd}t'_{pd}$ for 0.2 mm sand for flows with u=20 mm s^{-1} impacted by drops falling from various heights (F).

ANALYSIS FOR EFFECT OF FLOW DEPTH (h) ON $D_{pd}t'_{pd}$ LINEAR REGRESSION $D_{pd}t'_{pd} = k_0 - b_2h = k_0 (1 - \beta h)$									
F (m)	v_d ($m.s^{-1}$)	k_0 (mg.s)	std dev	b_2	std dev	β (mm^{-1})	h range	n	r^2
				d=2.7 mm					
1.0	4.05	2.774	0.067	0.417	0.015	0.1503	3.1-6.0	8	0.991
3.0	6.07	8.066	0.208	0.978	0.040	0.1237	3.1-7.2	8	0.989
11.2	7.61	12.289	0.438	1.332	0.078	0.1084	2.9-7.6	13	0.961
				d=5.1 mm					
1.0	4.24	22.873	0.743	1.520	0.095	0.0665	3.1-11.9	10	0.966
3.6	7.15	50.080	1.131	2.674	0.124	0.0534	3.1-11.8	12	0.977
11.2	8.95	[66.906]*		[3.388]*		[0.0506]*			
11.2	8.95	53.954	1.551	2.468	0.214	0.0457	3.1-12.6	10	0.936

* linear extrapolation from F=1m,3.6m data

FIG. 3.15

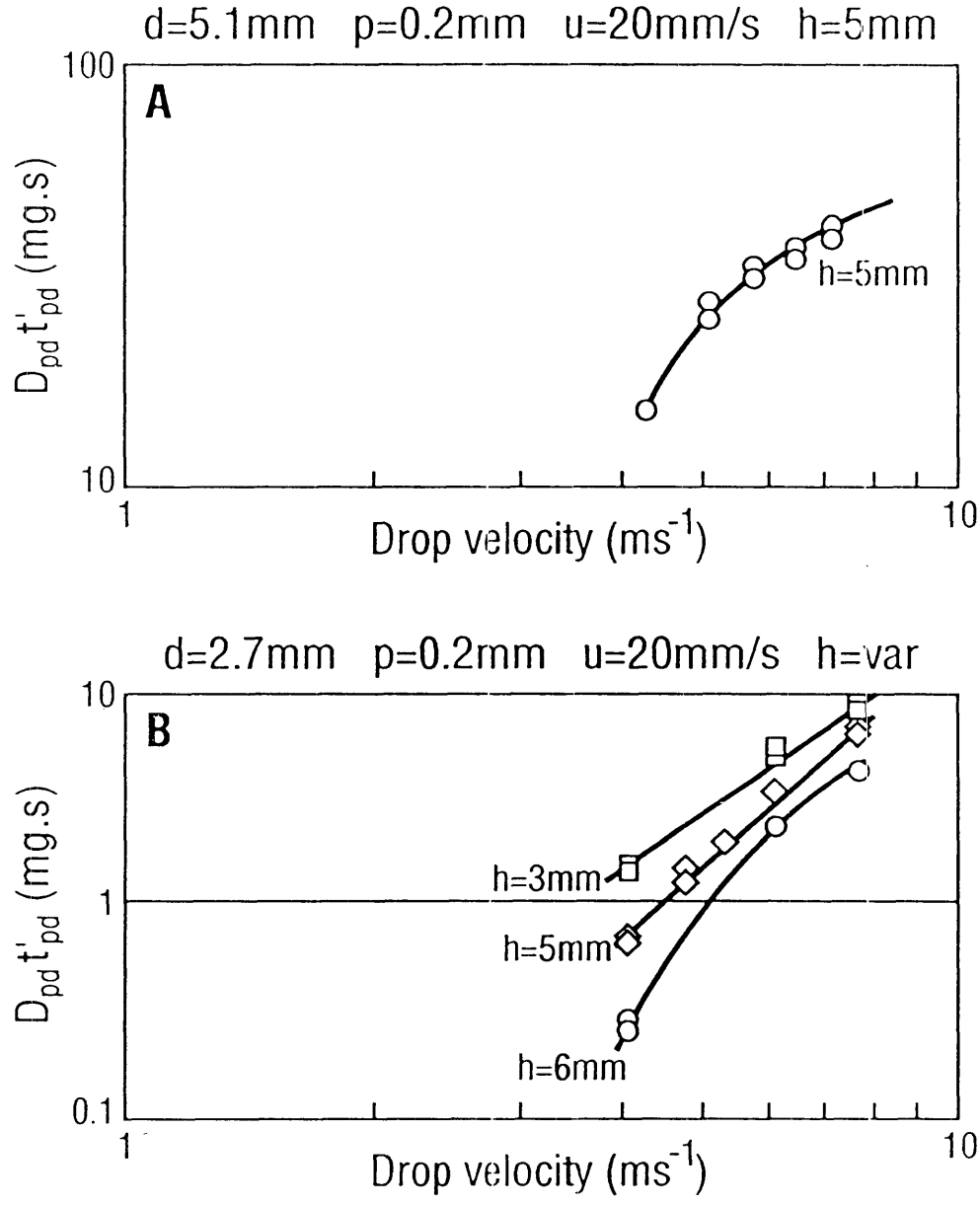

Figure 3.15. The effect of flow depth (h) on the relationship between $D_{pd}t'_{pd}$ and v_d for (A) 5.1 mm drops and (B) 2.7 mm drops.

and

$$\beta = 0.1104 - 0.001166\ p_m \qquad (3.15)$$

with r^2 values of 0.992 and 0.980, respectively.

3.3.5 *Particle density*

As noted in section 3.2.1, coal particles with a density 1.32 Mg m^{-3} (measured using the water displacement method) were used to determine the effects of changes in particle density. The fall velocities of the coal particles in water are given in Table 3.5.

Figure 3.16A shows the $D_{pd}t'_{pd}$ to h relationships for 0.2 mm sand and 0.46 mm coal particles transported by 2.7 mm drops. The fall velocities for the two particles are comparable (30 mm s^{-1} *cf* 24 mm s^{-1}) but the 0.46 mm particles of coal produce a value of k_0 that is some 3 times that of the 0.2 mm sand. In the case of 5.1 mm drops, the transport rates for the 0.46 mm coal when h>10 mm are about 4-5 times those of the 0.2 mm sand (Fig. 3.16B). However, for drops of this size, the peak in $D_{pd}t'_{pd}$ for the coal particles occurs when d<h<3d (Figs. 3.16B and 3.16C) rather than when h<d.

3.3.6 *Soil monoliths*

The results of experiments with sand and coal presented above are for conditions where the surface is covered completely by loose non-cohesive material and where single active zones are operating. In contrast, sediment with a wide range of particle size and density was discharged in the experiments using soil monoliths and, in many of the monoliths, the surface was observed to be free of loose material after the erosion experiments (Kinnell *et al.*, 1990). In these experiments, a large number of active zones operated simultaneously, and the degree of protection provided by pre-detached material (H, Chapter 2) was substantially different from one in many cases. However, as can be seen from Table 3.6, the effect of flow depth (h) on $D_{pd}t'_{pd}$ under these conditions follows the same form (Eq. 3.5) as observed for the experiments with uniform sized sand.

Table 3.5. Median terminal fall velocities in water (v_p in mm s^{-1}) for the particles used in the current experiments. These velocities were determined using the technique of Puri (1934) as described by Hairsine and McTainsh (1986).

p (mm)	sand	coal	ratio
0.11	10.5		
0.2	30	10	3.00
0.46	66	24	2.75
0.9	140	50	2.80
density (Mg m^{-3})	2.64	1.32	2.0

FIG. 3.16

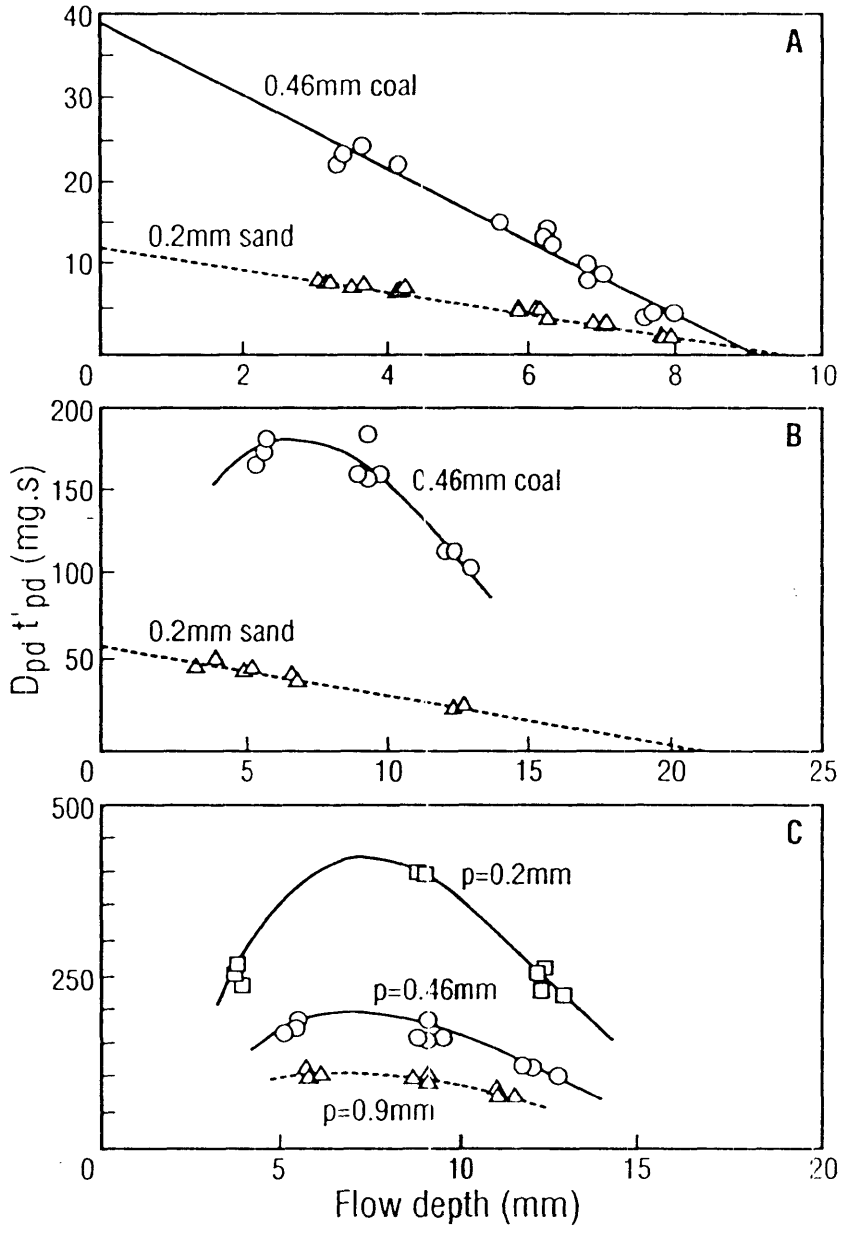

Figure 3.16. The $D_{pd}t'_{pd}$ to h relationships obtained for 2.7 mm (A) and 5.1 mm drops (B and C) impacting flows over coal particles. The relationships for 0.2 mm sand in (A) and (B) provide a comparison with particles with similar fall velocities to the 0.46 mm coal particles.

Table 3.6. Regression analysis for the effect of flow depth (h) on $D_{pd}t'_{pd}$ in the experiments with soil monoliths.

ANALYSIS FOR EFFECT OF FLOW DEPTH (h) ON $D_{pd}t'_{pd}$

NON-LINEAR REGRESSION $D_{pd}t'_{pd} = k_0 (1-\beta h)$

$\beta = 0.105$ se = 0.0029

Surface Type								
DEPOSITIONAL			RAIN-CAUSED CRUST			ORGANIC CRUST		
Plot No.	k_0	se	Plot No.	k_0	se	Plot No.	k_0	se
100	10.686	0.472	70	5.471	0.438	11	2.741	0.414
23	10.479	0.465	27	6.640	0.799	16	1.259	0.104
			12	12.375	0.588	58	2.376	0.459
			Ges	15.721	0.637	26	0.860	0.539
						51	2.640	0.435
						97	2.230	0.300
						63	1.961	0.465

97.8% variance accounted for

3.3.7 *Subsidiary experiments*

In addition to the main set of experiments which were designed to examine the effect of drop, particle and flow characteristics on $D_{pd}t'_{pd}$, a few subsidiary experiments were performed to (a) examine the manner in which particles moved from their initial point of detachment, and (b) examine the effect of particle fall velocity (v_p) on the effective average distance (x'_p) of particle travel.

A. *Dispersion of detached particles*

As noted in section 3.3.1, the upstream end of the sand target actively erodes because there is no sediment brought into this zone by the inflow. The material eroded from this zone moves downstream across the surface in the zone downstream of it and replenishes the sand removed from the downstream zone by previous impacts. This replenishment maintains the bed elevation in the downstream zones during the rainfall event. Attempts to label the 0.2 mm sand with a black cement colouring material (iron oxide) in order to trace the movement of the eroded sand were not particularly successful. However, a beach sand that did stain black with the cement colouring was obtained. This stained sand produced sediment transport rates which did not differ significantly from the 0.2 mm sand used previously.

Experiments with the 0.2 mm sand in a 85 mm by 500 mm source zone at the upstream end of the target, and the black sand in the remaining 415 mm by 500 mm zone, and vice versa, showed that the source sand did not move as a distinct wave. For h=5 mm, u=20 mm s^{-1}, 5.1 mm drops impacting at 7.15 m s^{-1} produced a sediment transport rate of 183 mg m^{-1} s^{-1}, and the sediment transported from the surface during 10 minutes, when spread about 0.5 mm thick, covered an area 70 mm by 500 mm. However, in the experiments, only an area about 25 mm wide showed any sign of being covered by a layer of source material a few particles thick (Fig. 3.17) and this layer thinned out to a single layer of particles by about 35 mm from the edge of the source zone. The concentration of the source particles then fell progressively until there was next to no visual evidence of these particles by 150 mm from the source.

FIG. 3.17

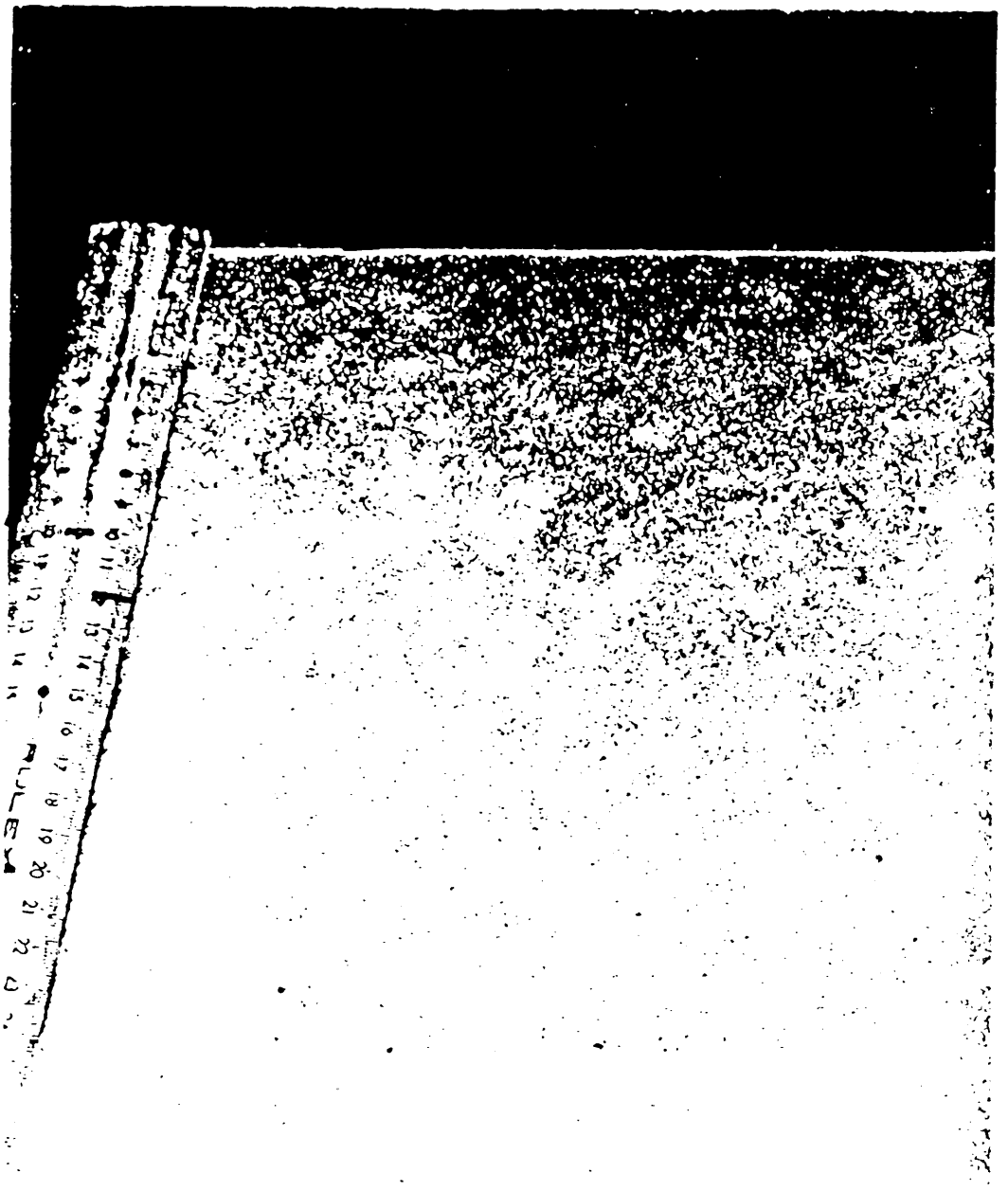

Figure 3.17. Photograph of the surface after an experiment in which a source zone of black sand (above end of ruler) was used at the upstream end of the target when 5.1 mm drops falling from 3.6 m impacted 5 mm deep flows where u=20 mm s^{-1} over 0.2 mm sand.

FIG. 3.17

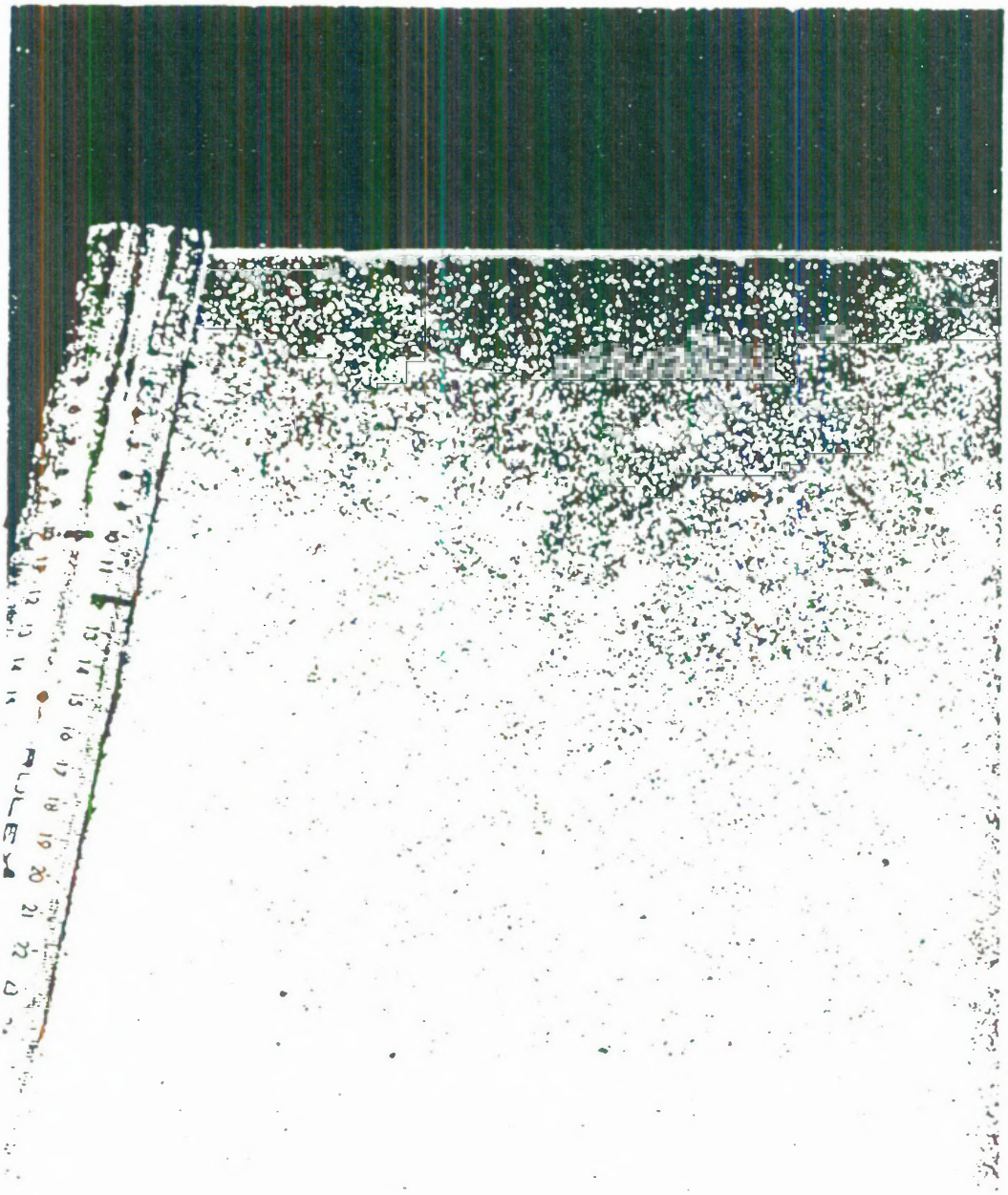

Figure 3.17. Photograph of the surface after an experiment in which a source zone of black sand (above end of ruler) was used at the upstream end of the target when 5.1 mm drops falling from 3.6 m impacted 5 mm deep flows where u=20 mm s^{-1} over 0.2 mm sand.

Scraping the surface away indicated that very little mixing of the source and the other sand occurred in the top 1 mm of the surface and there was certainly no evidence that mixing extended down to 2 mm below the surface.

Considering that a 25.4 mm wide strip of the downstream zone would have been impacted by about 1600 5.1 mm drops during the 10 minutes the target was exposed to the rain, there appears to be plenty of opportunity for the eroded material to be dispersed widely over the bed once it leaves its source area.

B. *Particle travel distances*

In the experiments designed to examine the effect of particle fall velocity (v_p) on the effective distance of particle travel (x'_p), the trough normally used as the sand trap was replaced by one with seventeen 25 mm-wide segments. A flat plate suspended 260 mm above the downstream end of the target at an angle to the direction of flow (Fig. 3.18.1) was used to protect the downstream end of the target so that, except for segments 16 and 17, particles entering any given segment had to have travelled a distance that was different to those entering neighbouring segments. The target area upstream of segments 16 and 17 was never protected in any way.

The general experimental procedure adopted was to expose a completely unprotected target for a period of time ranging from 0 to 8 minutes. Then, after a period of no rain in which the cover and the segemented trough were placed in their respective positions, the target was exposed to the rainfall for 2 minutes. The exposure time of 2 minutes was chosen so that the material deposited in the protected zone was not sufficient to cause major changes in the flow patter over the target.

Figure 3.18.2A shows the average amounts of material collected in each segment relative to segment 17 during 5 runs in which 2.7 mm drops impacted 7 mm deep flows over 0.46 mm sand. The pre-treatment (no cover) was varied over 0 to 8 minutes between the 5 runs. In addition to these five 2-minute runs where the downstream end of the target was screened, a 10-minute run using the segmented trough was done with a completely unprotected target in order to obtain a measure of the spatial variability of the sediment discharge in a normal experiment. The relative distribution obtained for this run is shown in

FIG. 3.18.1

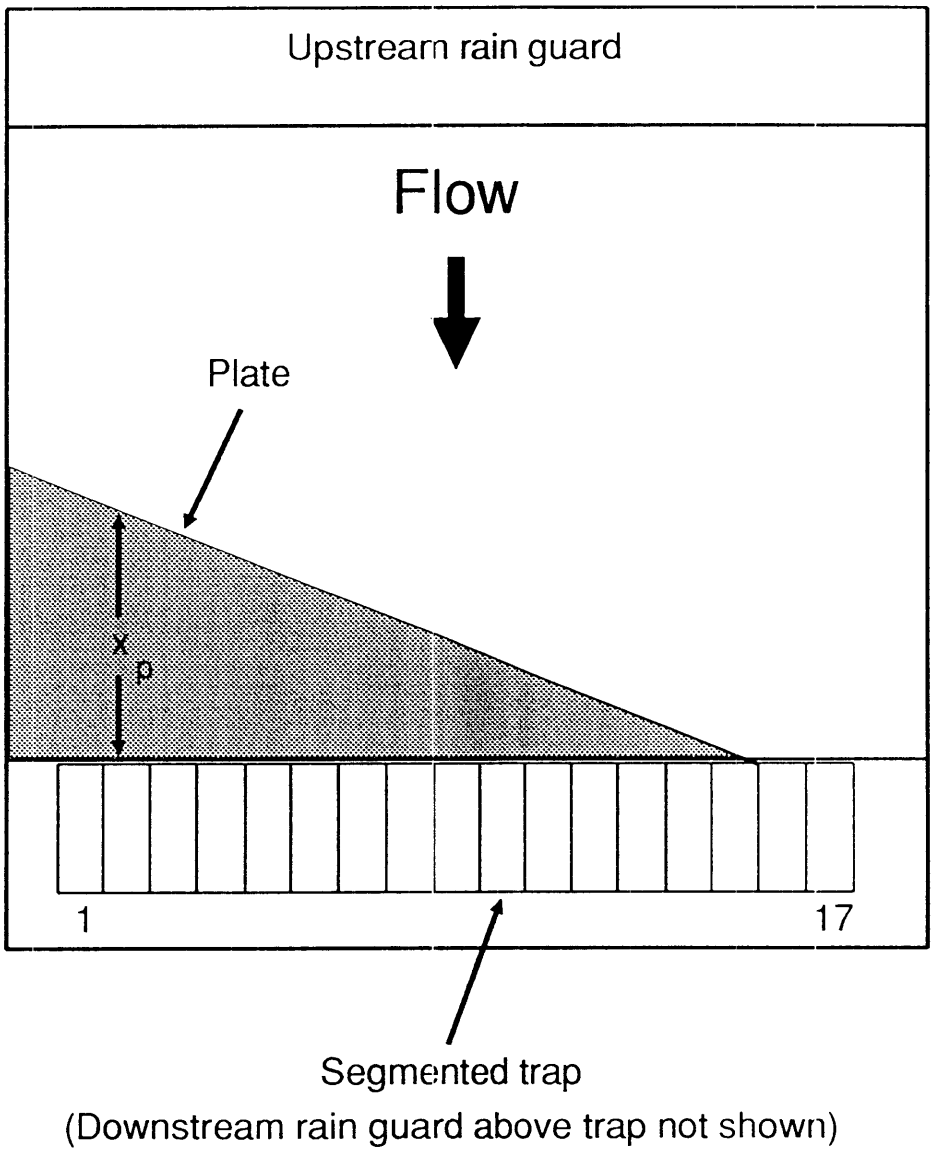

Figure 3.18.1. Schematic diagram (top view) of the arrangement used to protect the lower end of the target so as to restrict the source area for material entering specific segments when a segmented sand trap was used in the experiments. The angled plate was attached to the rain guard above the sand trap (Fig. 3.4) and restricted the rain application area over the downstream end of the target by various amounts in the cross flow direction.

FIG. 3.18.2

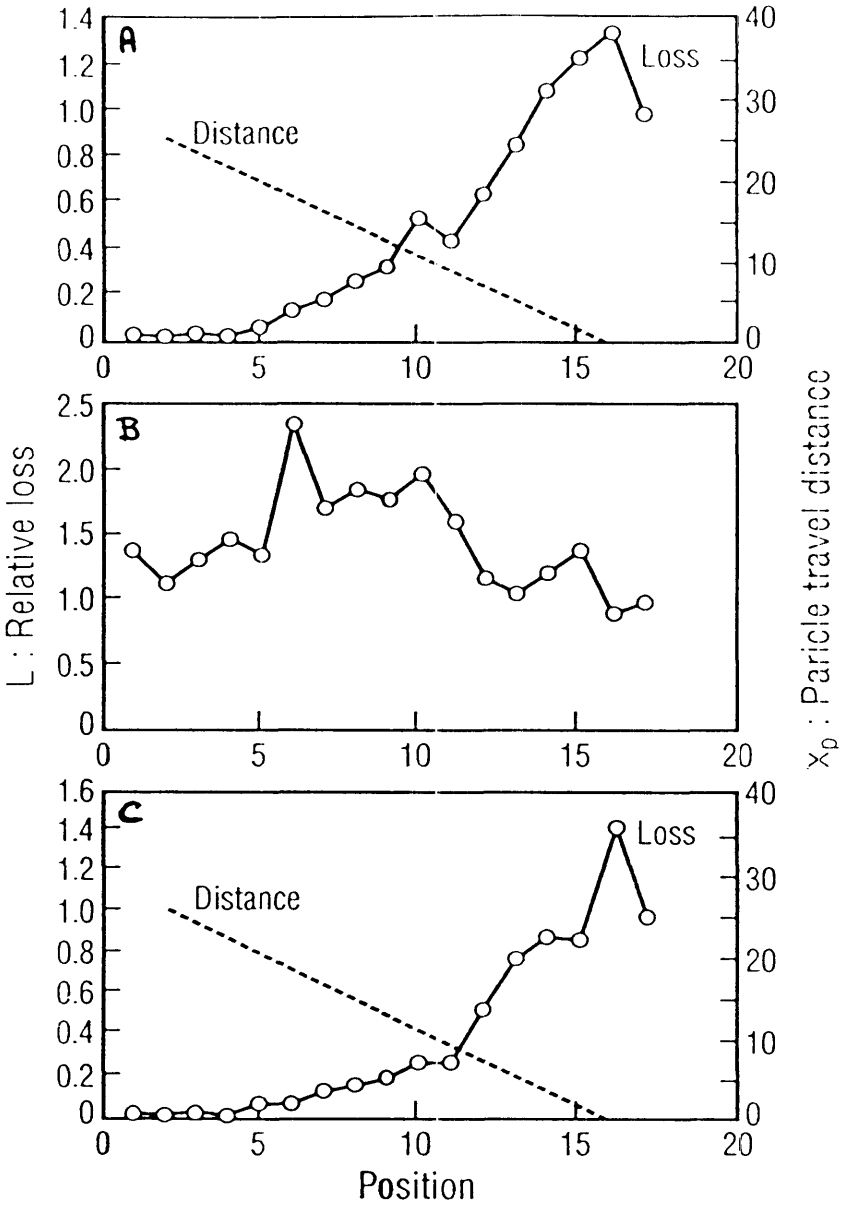

Figure 3.18.2 The distribution of the sediment discharged across the downstream boundary into a segmented trough observed (A) when downstream end of a target of 0.46 mm sand was covered by an angled plate and (B) in a normal experiment when 7 mm deep flows with u=40 mm s^{-1} were impacted by 2.7 mm drops at 64 mm h^{-1}. L is the loss relative to segment 17 which always collected material from an unprotected zone. (C) shows (A) corrected for the non-uniformity of the discharge shown in (B). The distance of particle travel associated with each segment is also shown in (A) and (C).

Fig. 3.18.2B. Because the spatial distribution of the sediment discharge was not uniform under normal conditions, the spatial distribution obtained when the downstream end of the target was protected was biased in certain segments. Fig. 3.18.2C shows the distribution that results when the data in Fig. 3.18.2B was used to correct for this bias.

From the data shown in Fig. 3.18.2C, data on the relative loss (L) as particle travel distance (x_p) varies can be obtained. From Eqs. 2.12 and 2.19, it follows that the effective average particle travel distance (x'_p) is given by

$$x'_p = \frac{\sum_{n=1}^{15} (L_n . x_{pn})}{L_m} \qquad (3.16)$$

where L_m is the mean value of L observed for the 15 segments with $x_p>0$. Applying Eq. 3.16 to the data for the 2.7 mm drops impacting 7 mm deep flows over 0.46 mm sand gives x'_p = 6.05 mm. For the same drop and flow conditions over 0.46 mm coal, x'_p = 18.36, 3.03 times the value of x'_p calculated for the 0.46 mm sand. Since this is of a similar magnitude to the ratio of the values of v_p (2.75, Table 3.5) and to the ratio of the values of k_0 (3.95, 38.54 mg.s (Fig. 3.16) to 9.75 mg.s (Table 3.3B)), it would appear that most of the variation in $D_{pd}t'_{pd}$ between 0.46 mm sand and 0.46 mm coal in flows impacted by 2.7 mm drops results from variations in t'_{pd} rather than variations in D_{pd}.

3.4 DISCUSSION

The relationship between $D_{pd}t'_{pd}$ and h for d<h<3.5d for medium-to-large drops is given by Eq. 3.5. Because k_0 is influenced by both particle characteristics and drop characteristics and ß by only drop characteristics, it is appropriate to rewrite Eq. 3.5 as

$$D_{pd}t'_{pd} = k'_{pd} (1 - ß_d h) \qquad (3.17).$$

where $ß_d = h_d^{-1}$ and h_d is the projected value of h for $D_{pd}t'_{pd} = 0$. The analyses producing Eqs. 3.10 and 3.14 show the effects of d and p to be multiplicative rather than additive so that Eq. 3.17 can be rewritten as

$$D_{pd}t'_{pd} = k'_p k'_d (1 - \beta_d h) \qquad (3.18).$$

In RIFT, the uplift of particles from the underlying surface results as a reaction to a stress applied on that surface during drop impact. Gilley *et al.* (1985) suggest that the erosive stress applied by drops impacting a flow might be related to the peak pressures (P_{max}) measured by Wenzel and Wang (1970). However, $D_{pd}t'_{pd}$ is only linearly related to P_{max} over a limited range of P_{max} (Fig. 3.19).

Usually a critical force needs to be overcome before particles are lifted from the bed into the flow. In such circumstances, a linear relationship between $D_{pd}t'_{pd}$ and $X - X_c$ (where X is a parameter directly related to stress applied to the bed by the impacting drop and X_c is the value of that parameter when the critical stress occurs) is to be expected. The increase of β_d with d and v_d may be thought to result from such a critical stress. However, in the experiments where particle size was varied, β_d was not influenced by the changes in particle size (Fig. 3.11, Table 3.3). The experiments with soil monoliths also show that the β_d is not influenced by factors, such as cohesion and interparticle friction, which influence the ability of soil surfaces to yield particles to the transport mechanism. The value of β_d obtained when H≠1 for 2.7 mm drops impacting flows over the soil surfaces (Table 3.6) is the same as the value of β_d obtained for 2.7 mm drops impacting flows over beds of non-cohesive materials (H=1) after falling from the same height (Table 3.3). Evidently the complexities of the processes that occur during a drop impact are such that the results cannot be explained in terms of simple physics when h<3d. The use of high speed photography (e.g., Ghadiri and Payne, 1979; Cai, 1989) and computer models based on the Navier-Stokes equations (e.g., Harlow and Shannon, 1967; Ferreira *et al.*, 1985) may facilitate better understanding of the processes involved when h<3d. However, this approach is beyond the scope of this present study.

In terms of sediment transport by flowing water, the fall velocity (v_p) of a particle in water is considered to be a single integrating factor accounting for the effects of particle size, shape and density (Loch, 1989). In the experiments using non-cohesive beds (H=1), k_0, and hence k'_p, varied inversely with v_p to a power of -0.46 in the case of sand (Eq. 3.10, Fig. 3.13). Also, changes in particle density caused major variations in $D_{pd}t'_{pd}$

FIG. 3.19

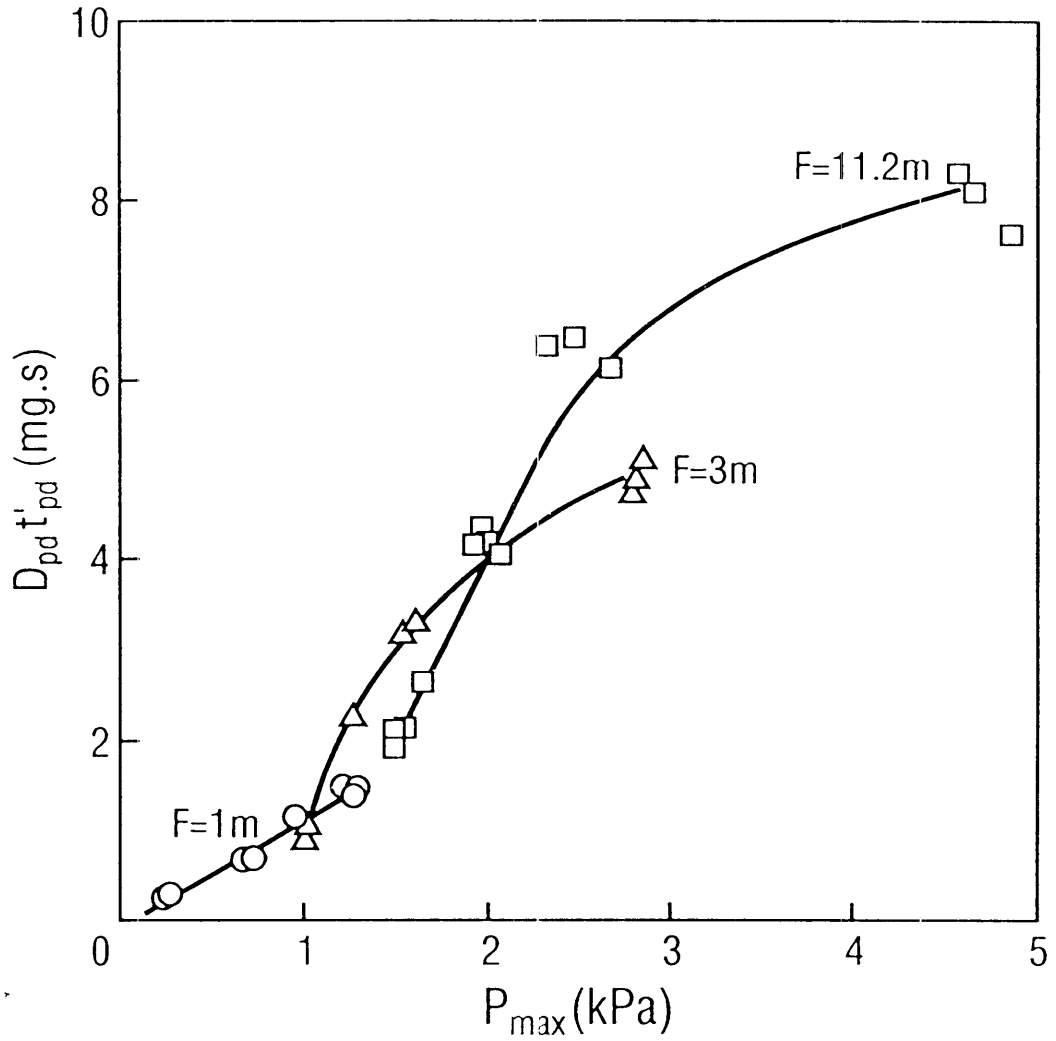

Figure 3.19. The effect of P_{max} on $D_{pd}t'_{pd}$ for 2.7 mm drops impacting flows over 0.2 mm sand after falling from various heights (F). The values of P_{max} used result from Fig. 3.2 and the observation by Wenzel and Wang (1970) that P_{max} varies directly with the square of drop impact velocity.

when v_p remained relatively constant (Figs. 3.16A and 3.16B) despite evidence that variations in x'_p between 0.46 mm sand and 0.46 mm coal in flows impacted by 2.7 mm drops were of the magnitude expected from the variations in v_p between these two materials (Section 3.3.7(B)). Evidently, the effect of v_p on $D_{pd}t'_{pd}$ depends on whether particle size or density varies (Fig. 3.20) so that the concept of using particle fall velocity to determine the effective "size" of sediment particles may not be useful on its own in the context of RIFT.

From Eqs. 2.20, 2.22 and 3.18, the sediment transport rate (q_{sR}) and concentration (c_R) can be expressed by

$$q_{sR}\,[p,d] = \frac{6\,R_d\,u\,k'_p k'_d[1 - \beta_d h]}{\pi\,d^3} \qquad (3.19),$$

and

$$c_R\,[p,d] = \frac{6\,R_d\,k'_p k'_d[h^{-1} - \beta_d]}{\pi\,d^3} \qquad (3.20)$$

respectively. For drops impacting flows over sand at close to their terminal velocities, k'_p varies with p to a power -0.62 (Eq. 3.9) or v_p to a power of -0.46 (Eq. 3.10). k'_d varies with d to a power of 2.24 (Eqs. 3.9 and 3.10) or drop momentum (p_m) to a power of 0.70 under these conditions while β_d is linearly related to both d (Eq. 3.8) and p_m (Eq. 3.12).

It follows from Eq. 3.19, that the effects of the raindrop, flow and soil factors can be represented by an equation of the form

$$q_{sR}[p,d] = k_s\,R\,u\,f[h,d] \qquad (3.21)$$

where k_s accounts for the susceptibility of the surface to erosion by rain-impacted flow and the function $f[h,d]$, which varies between 0 and 1, accounts for the drop size - flow depth interaction. When coupled with the explicit effect of drop mass in Eq. 3.19 ($\pi d^3/6$), the effect of drop size on k'_d noted above ($k'_d \alpha d^{2.24}$) for drops travelling at close to their terminal velocities results in the q_{sR} to h relationships converging towards a common value of q_{sR}

FIG. 3.20

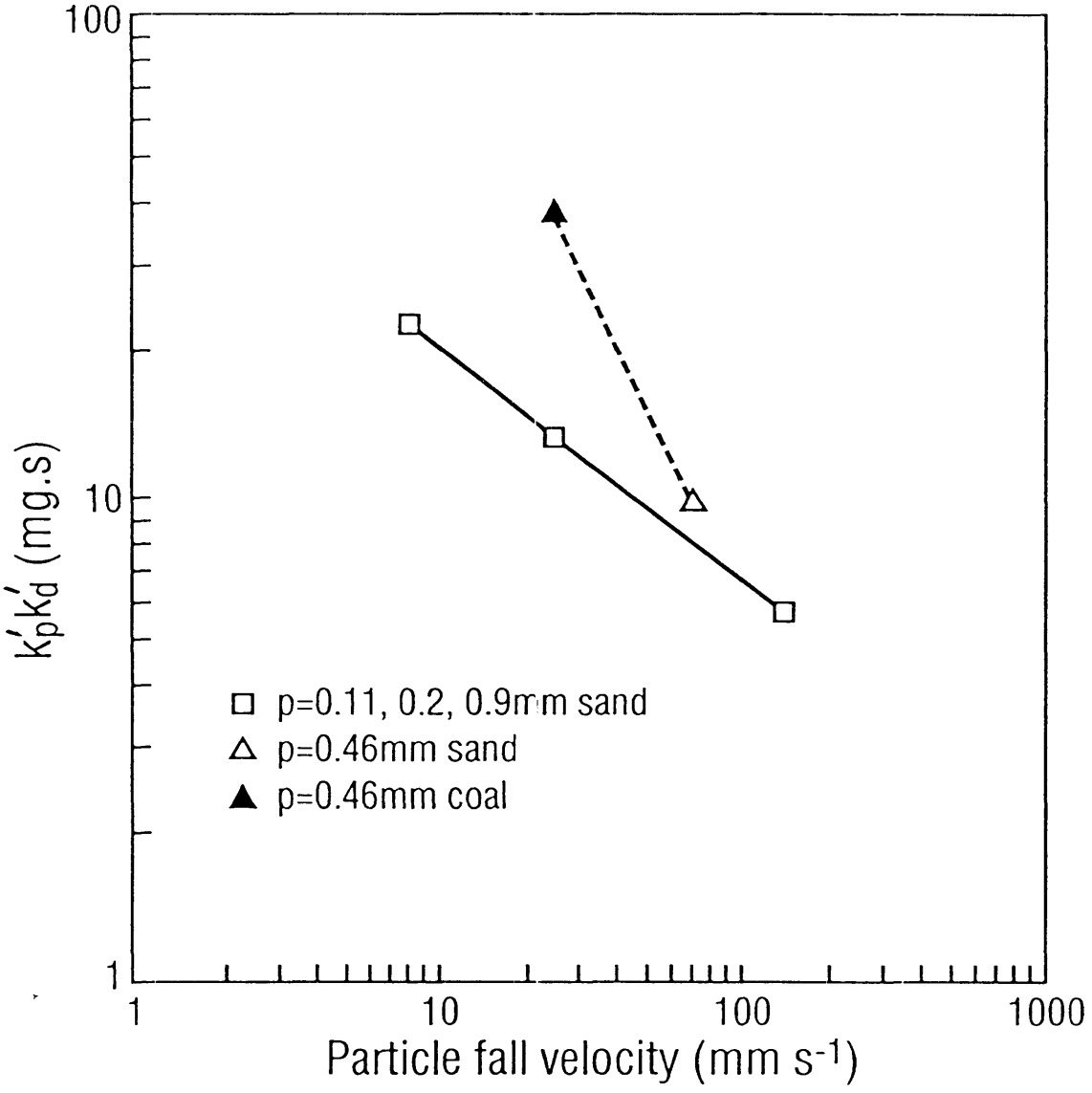

Figure 3.20. The effect of particle fall velocity (v_p) on $k'_p k'_d$ for 2.7 mm drops impacting flows over sand and coal particles.

at about h=4 mm for the rainfall conditions studied (Fig. 3.21). Under these circumstances,

$$f[h,d] \approx 1-\beta_d[h-h_x] \quad , h_x<h<3d \quad (3.22)$$

where h_x is the value of h where the common value of q_{sR} occurs. From the experiments with sand,

$$\beta_d = 0.3119 - 0.0507d \quad , r^2=0.985 \quad (3.23)$$

and Eqs. 3.21 - 3.23 account for 97.6% of the variance in q_{sR} when h_x=4.08 mm.

Equation 3.22 is an approximation that results from the current experiments. It indicates that raindrop size does not have a significant influence on q_{sR} when medium-to-large drops impact flows that are less than 4 mm deep. The results of the experiments of Walker *et al.* (1978) with 1-3 mm deep flows on 3 m long planes of sand inclined at 5 % provide evidence to support this. The lack of effect of drop size appears to result from the water surface providing a major restriction on the height to which particles can be lifted when high energy raindrops impact shallow flows. As shown in Figs. 3.22 and 3.23, flow depth has an effect on q_{sR} when medium-to-large drops travelling at subterminal velocity, and small drops travelling at terminal velocity, impact flow shallower than 4 mm.

It follows from Eq. 3.21 that

$$k_s\ f[h,d] = \frac{q_{sR}[p,d]}{R\ u} \quad (3.24).$$

Analysis of data such as that shown in Fig. 3.9 indicates that $k_s\ f[h,d]$ varies with the product of h and an exponential function of h. Figures 3.24 and 3.25 show the relationships between log ($k_s\ f[h,d]\ h^{-1}$) and h obtained when Eq. 3.24 is applied to the data for p=0.2 mm obtained in the current experiments and the experiments of Moss and Green (1983). These figures indicate that the relationship between $k_s\ f[h,d]\ h^{-1}$ and exp(h) for d=5.1 mm provides a reasonable estimate of the effect of flow depth when flow depth wholly constrains q_{sR}, and that, when flows are deeper than a critical flow

FIG. 3.21

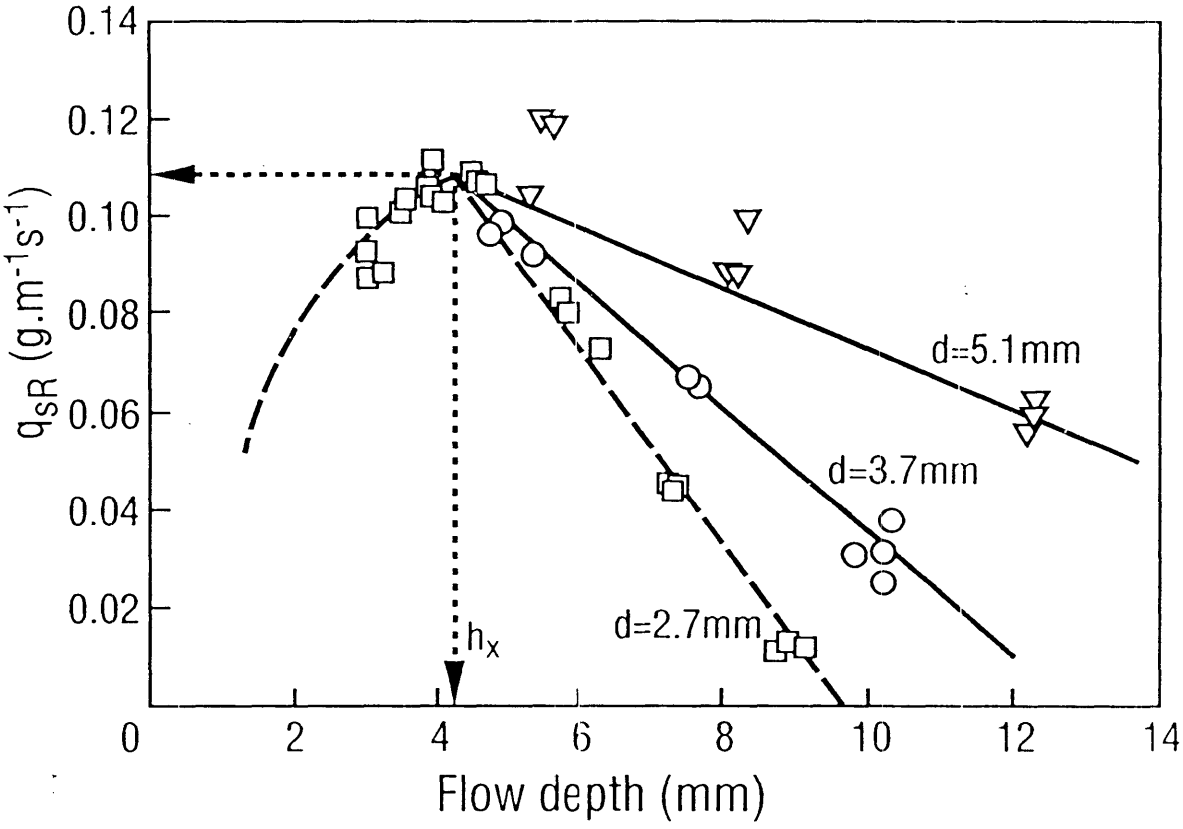

Figure 3.21. The effect of drop size on the relationship between sediment discharge and flow depth for flows over 0.9 mm sand. h_x is the depth of flow where q_{sR} is common for the three linear relationships between q_{sR} and flow depth (h) shown.

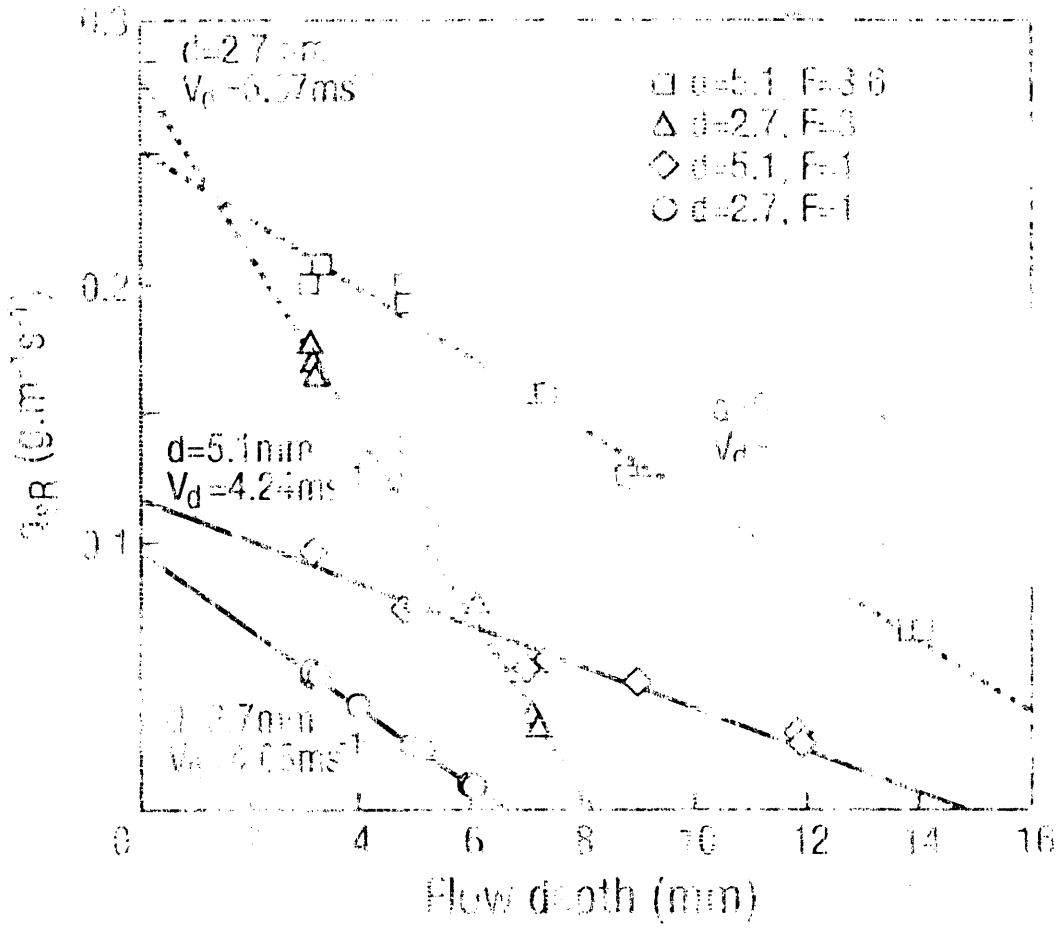

Figure [illegible] The effect of drop impact velocity on the relationship between splashed discharge and flow depth for [illegible]

FIG. 3.22

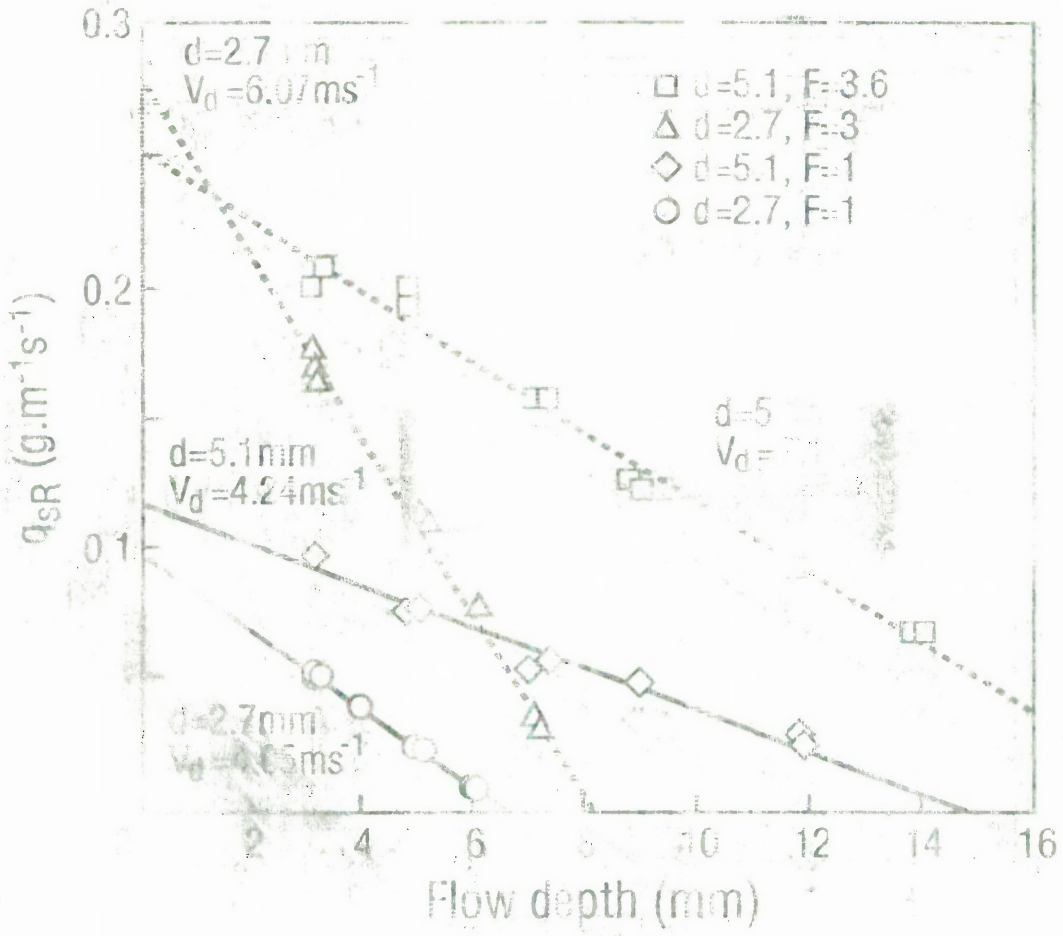

Figure 3.22. The effect of drop impact velocity on the relationship between sediment discharge and flow depth for flows over 0.2 mm sand

FIG. 3.23

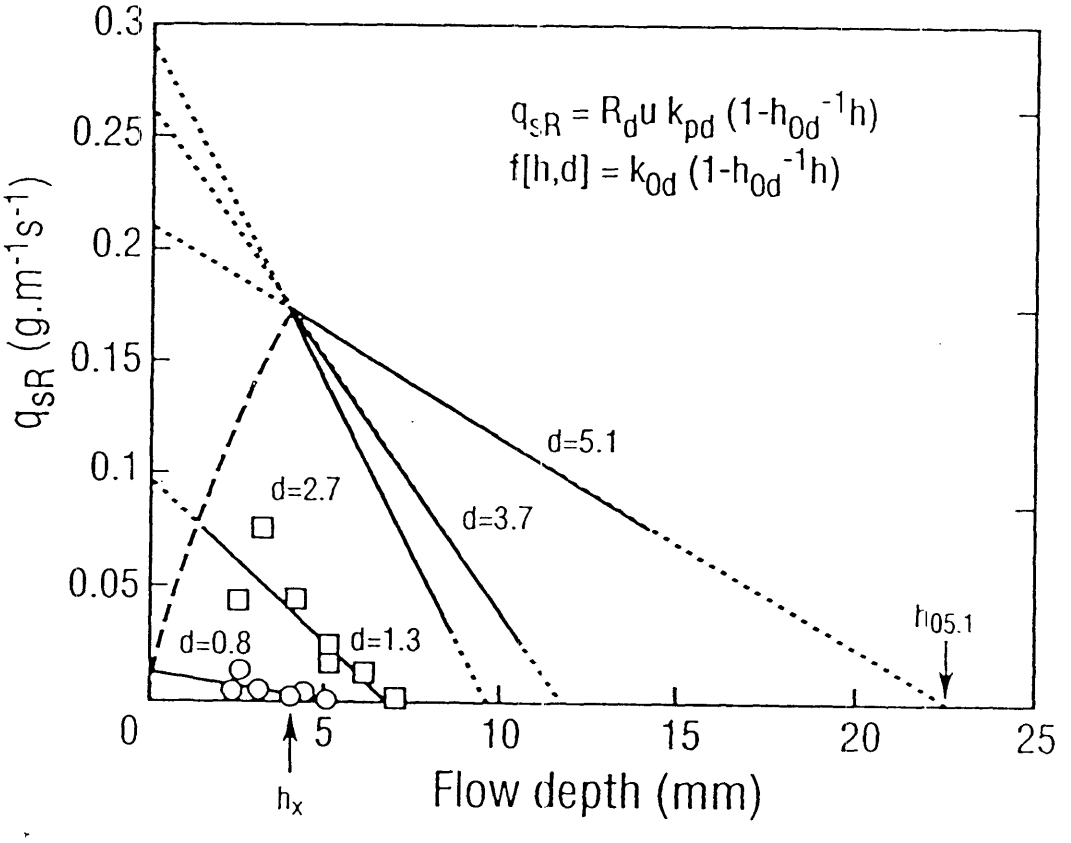

Figure 3.23. The effect of flow depth on q_{sR} for 0.2 mm sand for flows impacted by 0.8 mm and 1.3 mm drops in the experiments of Moss and Green (1983) together with the q_{sR}-h relationships that result for d≥2.7 mm from Eq. 3.21.

FIG. 3.24

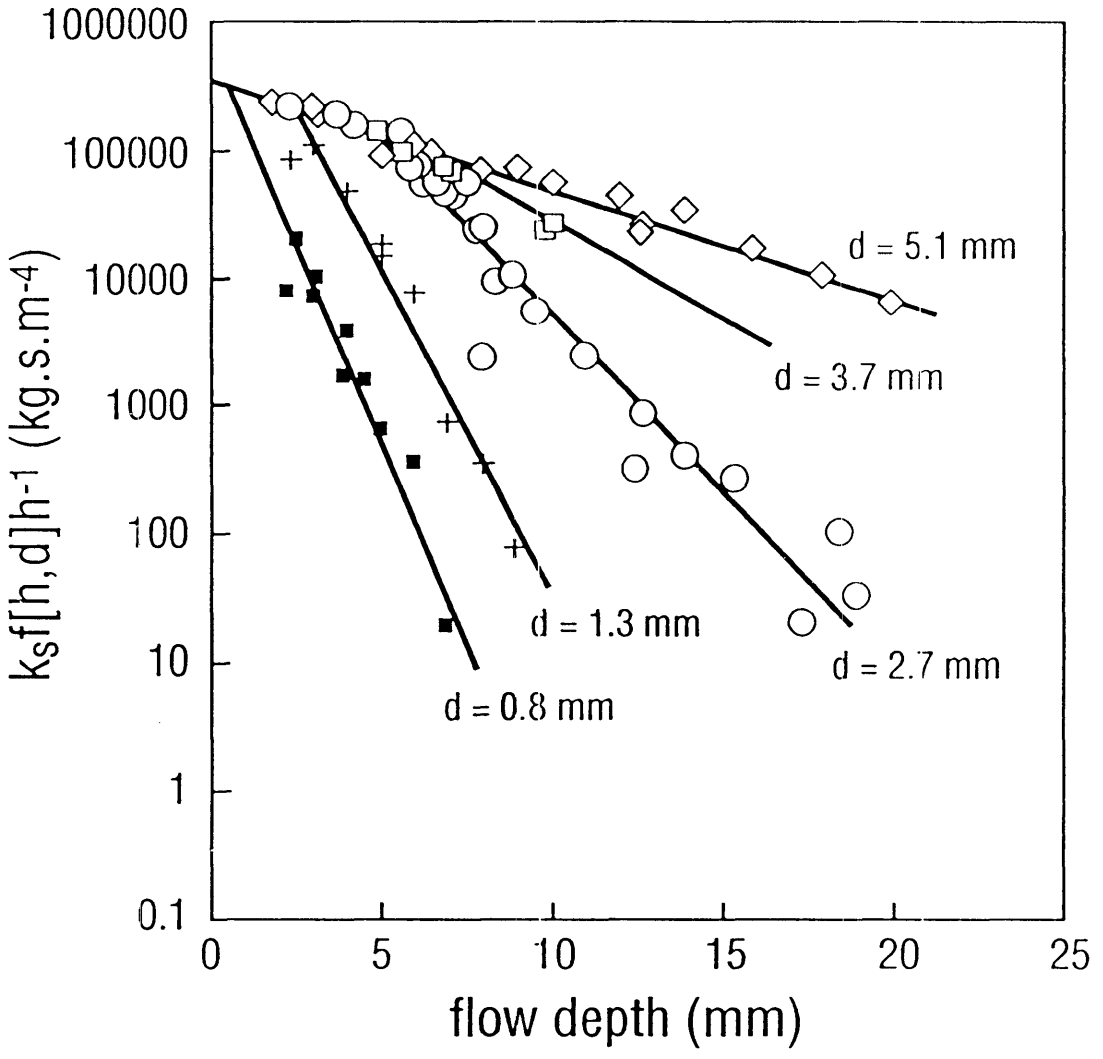

Figure 3.24. The relationships between k_s $f[h,d]h^{-1}$ and flow depth (h) for various sized drops in the current and Moss and Green (1983) experiments with drops travelling at or near terminal velocity impacting flows shallower than 21 mm. The data for h<11 mm is shown in greater detail in Fig 3.25

FIG. 3.25

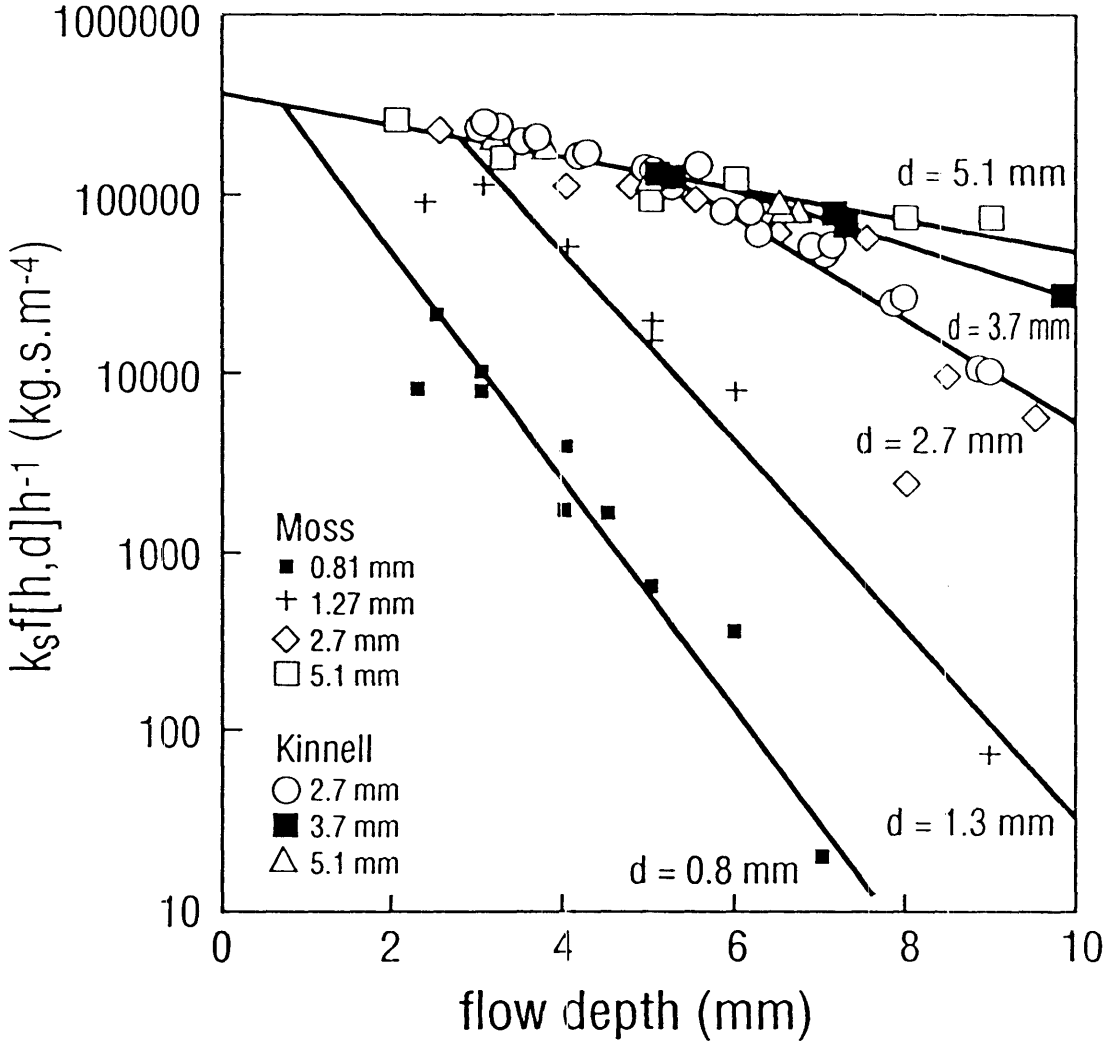

Figure 3.25. Greater detail of the data for the relationships between $k_s f[h,d]h^{-1}$ and flow depth (h) for various sized drops in the current and Moss and Green (1983) experiments with drops travelling at or near terminal velocity impacting shallow flows.

depth (h_c), the stress applied by the drop impact becomes the limiting factor. For the data shown in Figs. 3.24 and 3.25,

$$h_c = 1.74768 + 2.88237 \log(d) \qquad (3.25)$$

and

$$k_s f[h,d] = h \exp[5.7975 - 0.1881h] \qquad ,h \leq h_c \quad (3.26a)$$

$$k_s f[h,d] = h \exp[5.7975 - 0.1881h_c - b'_d(h - h_c)] \qquad ,h > h_c \quad (3.26b)$$

where

$$b'_d = \exp[0.76649 - 0.48251\, d] \qquad (3.27)$$

This model accounts for 97.7% of the variance in the data shown in Fig. 3.24. $f[h,d] = 1.0$ when Eq. 3.26a produces its peak value of 644 kg.s m^{-3} when h=5.3 mm so that, for 0.2 mm sand, k_s=644 kg.s m^{-3}. The corresponding values of k_s for the other materials used in the experiments are given in Table 3.7.

Fundamental to the theory leading to Eq. 3.12 is the concept that the sediment discharged across any given boundary results from the integrated effect of the drop impacts within the active zones associated with that boundary. Thus, given N drop sizes in a rainfall,

$$q_{sR}[s,r] = k_s \, R \, u \, f[h,r] \qquad (3.28)$$

where

$$f[h,r] = \frac{\sum_{n=1}^{N} (f[h,d]R_d)_n}{\sum_{n=1}^{N} (R_d)_n} \qquad (3.29)$$

and s and r denote the influence of soil and rainfall characteristics rather than particle size and drop size *per se*.

Table 3.7. k_s values and their coefficients of variation (CV) for surfaces under flows impacted by 2.7 mm drops falling from 11.2 m

H→1			H<<1		
p	k_s (kg.s m^{-3})	CV (%)	p	k_s (kg.s m-3)	CV (%)
-------loose material--------			-------rain-caused crusts----		
0.11mm sand	1106	5.5	Plot 70	281	7.6
0.2 mm sand	644	3.2	Plot 27	324	12.0
0.46mm sand	541	3.0	Plot 12	603	4.7
0.9 mm sand	281	2.1	Ges	767	4.0
0.46mm coal	1880	3.9			
----depositional material----			-------organic crusts--------		
Plot 100	521	4.4	Plot 11	134	15.1
Plot 23	510	4.4	Plot 16	62	8.3
			Plot 58	117	19.3
			Plot 26	42	62.7
			Plot 51	139	16.5
			Plot 97	109	13.4
			Plot 63	95	23.7

Equations 3.24-3.29 provide a mechanism for determining the effects of the interactions between raindrops, flow and the eroding surface on erosion by rain-impacted flow when raindrop and flow characteristics are known. Hairsine (1988) used artificial rainfall produced by nozzles situated 8 m above 5.8 m long planes of soil. Figure 3.26A shows the $f[h,r]$ to flow depth relationship that results from applying Eqs. 3.25-3.29 to the drop-size distribution measured by Hairsine while Fig. 3.26B shows the relationship between q_{sR} and $f[h,r]$ for the flow depths used by Hairsine (3 mm, 5 mm) when R=56 mm per hour and u=20 mm s^{-1}. Re-arranging Eq. 3.28 gives

$$k_s = \frac{q_{sR}[s,r]}{R\ u\ f[h,r]} \qquad (3.30)$$

and thus, from the data shown in Fig. 3.26, it follows the values Solonchak and Black Earth soils used by Hairsine had k_s values of 2567 kg.s.m^{-3} and 325 kg.s.m^{-3} respectively. The k_s for the Solonchak soil is greater than any of those obtained in the current experiments (Table 3.7).

3.5 SUMMARY

The ability of raindrops to induce sediment transport in shallow flow varies with a number of factors one of which is flow depth (h). For medium-to-large drops (d>2.0 mm), there are three regimes. The first appears to operate in very shallow flows when aerial splash is a major phenomenon. The third appears to operate when $h>h_2$ and h_2=3d. At h>3d, the collapse of above-water structures is the primary factor that leads to particles being lifted from the bed. The second regime appears to operate when h<3d and aerial splash is not a major factor in promoting sediment transport.

In the second regime, the sediment transport rate decreases linearly with flow depth over the range $h_1<h<h_2$ where h_1>3 mm. The projected intercept with the q_{sR} axis for this relationship is directly related to k_0 in Eq. 3.5. This intercept varies with drop size, drop velocity, particle size and cohesion. The projected intercept on the h axis, which is directly related to β^{-1}, is influenced by drop size and velocity but it is not influenced by particle size. Neither is it influenced by cohesion. It follows from these

FIG. 3.26

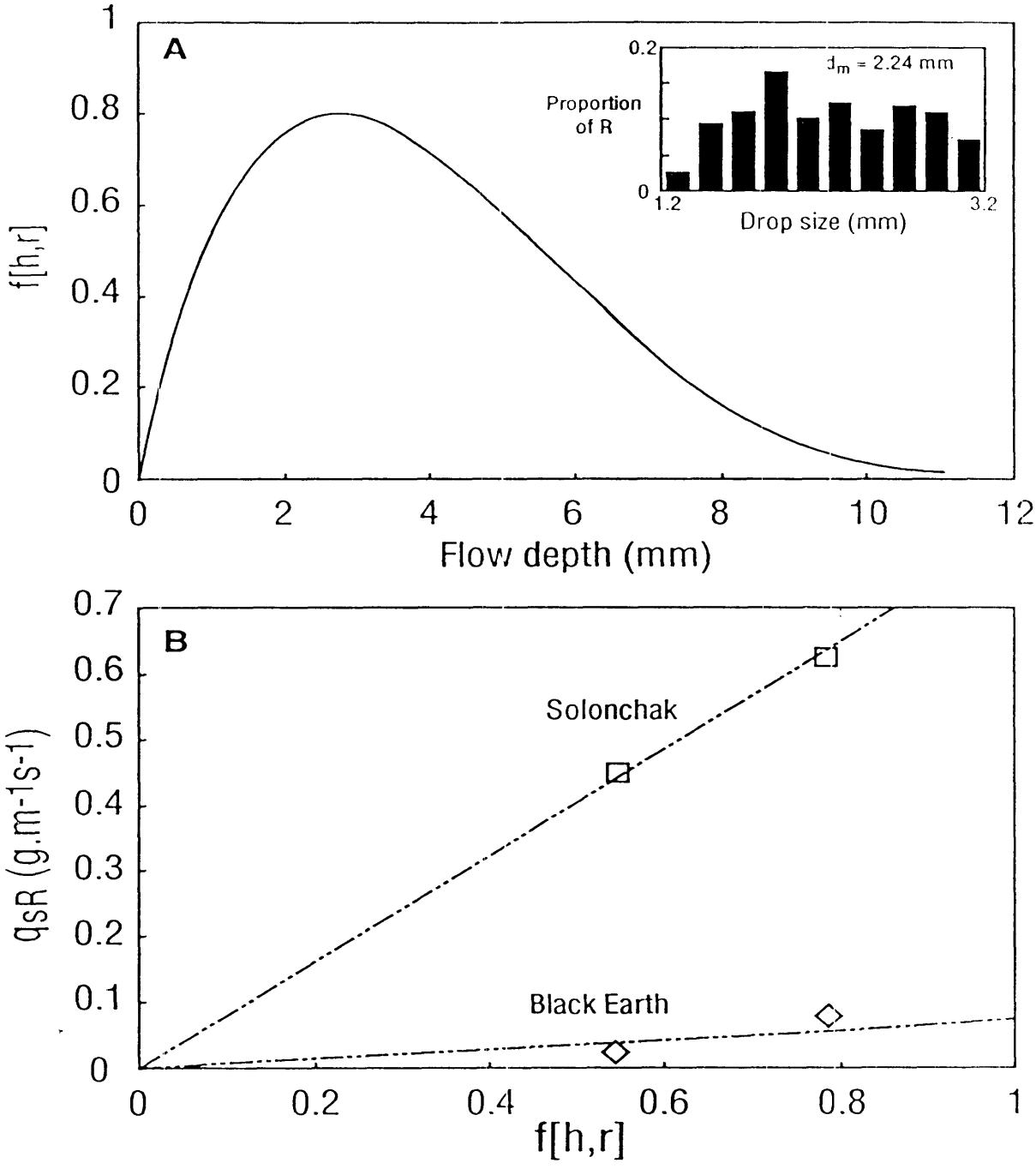

Figure 3.26. (A) the relationship between f[h,r] and flow depth (h) resulting from applying Eqs. 3.25 - 3.29 to the drop size data of Hairsine (1988) and (B) the relationship between the values of f[h,r] that result from Eqs. 3.25 - 3.29 and the q_{sR} values obtained for the two soils used by Hairsine when R=56 mm h^{-1} and u=20 mm s^{-1}.

results that, for the majority of particles moved by RIFT in the second regime, the effects of the various factors on the sediment transport rate (q_{sR}) and concentration (c_R) can be expressed by

$$q_{sR}\ [p,d] = \frac{6\ R_d\ u\ k'_p k'_d [1 - \beta_d h]}{\pi\ d^3} \qquad \text{for } h_1<h<h_2 \quad (3.19),$$

and

$$c_R\ [p,d] = \frac{6\ R_d\ k'_p k'_d [h^{-1} - \beta_d]}{\pi\ d^3} \qquad \text{for } h_1<h<h_2 \quad (3.20)$$

respectively. β_d is linearly related to both d (Eq. 3.8) and p_m (Eq. 3.12) but is not influenced by particle characteristics or factors such as cohesion. For sand, k'_d varies with d to a power of 2.24 (Eqs. 3.9 and 3.10) or drop momentum (p_m) to a power of 0.70. k'_p varies with p to a power -0.62 (Eq. 3.9) or v_p to a power of -0.46 (Eq. 3.10). However, contrary to popular belief, particle fall velocity does not appear to integrate the effects of particle size, shape and density well in RIFT.

Equation 3.19 can be rewritten as

$$q_{sR}\ [p,d] = k_s\ R_d\ u\ f[h,d] \qquad (3.21)$$

where $f[h,d]$ is a function accounting for the drop size - flow depth interaction. In Eq. 3.21, k_s provides a measure of the susceptibility of the eroding surface to erosion by rain-impacted flow because all the other terms account for the erosiveness of the rain-impacted flow. For $h_x<h<h_2$,

$$f[h,d] \approx 1 - \beta_d(h-h_x) \qquad (3.22)$$

but the convergence to a common value of q_{sR} as h decreases towards h_x indicates that, for flows shallower than h_x, raindrop size has a non-significant influence on the erosion rate when medium-to-large raindrops impact shallow flows. The data of Walker *et al.* (1978) for inclined planes of sand where flow depths varied between 1 and 3 mm are consistent with this conclusion but there is experimental evidence (Fig. 3.23) to indicate that raindrop characteristics continue to influence the erosion rate when small raindrops impact flows shallower than 4 mm. Combining the results obtained in

the current experiments with the data of Moss and Green (1983) yield a series of equations (Eqs. 3.25-3.29) that provide the means for determining the interactions between raindrops, flow and the eroding surface for rain over a wide range of flow depth.

Cohesion was not studied quantitatively here. However, results from the experiments with soil monoliths show quite clearly that cohesion has some influence on k_s. As indicated by the theory discussed in Chapter 2, the effect of cohesion on erosion by rain-impacted flows is not as direct as many may suppose and thus it remains a matter for future study.

In the experiments reported here, the frequency of the drop impacts was such that the whole of the uplift and deposition event associated with a drop impact tended to be separated temporally and spatially from other drop impacts. Under these conditions the mass of the particulate material in the flow above the active zone at any given time varies considerably in time and space. Thus, it is probable that, within the context of RIFT, sediment concentration should be considered as simply the mass of sediment discharged per unit mass or volume of water, not the mass of sediment dispersed in a unit mass or volume of the water flowing over the bed. Also, the approach which considers the direct effects of the detachment and deposition process on q_{sR} rather than c_R eliminates the need to consider the effect that q_w being directly related to flow depth (Eq. 2.18) has on c_R. In the approach used here, the effect that flow depth has on the material that is mobilised in RIFT is more readily identified than in approaches based on c_R.